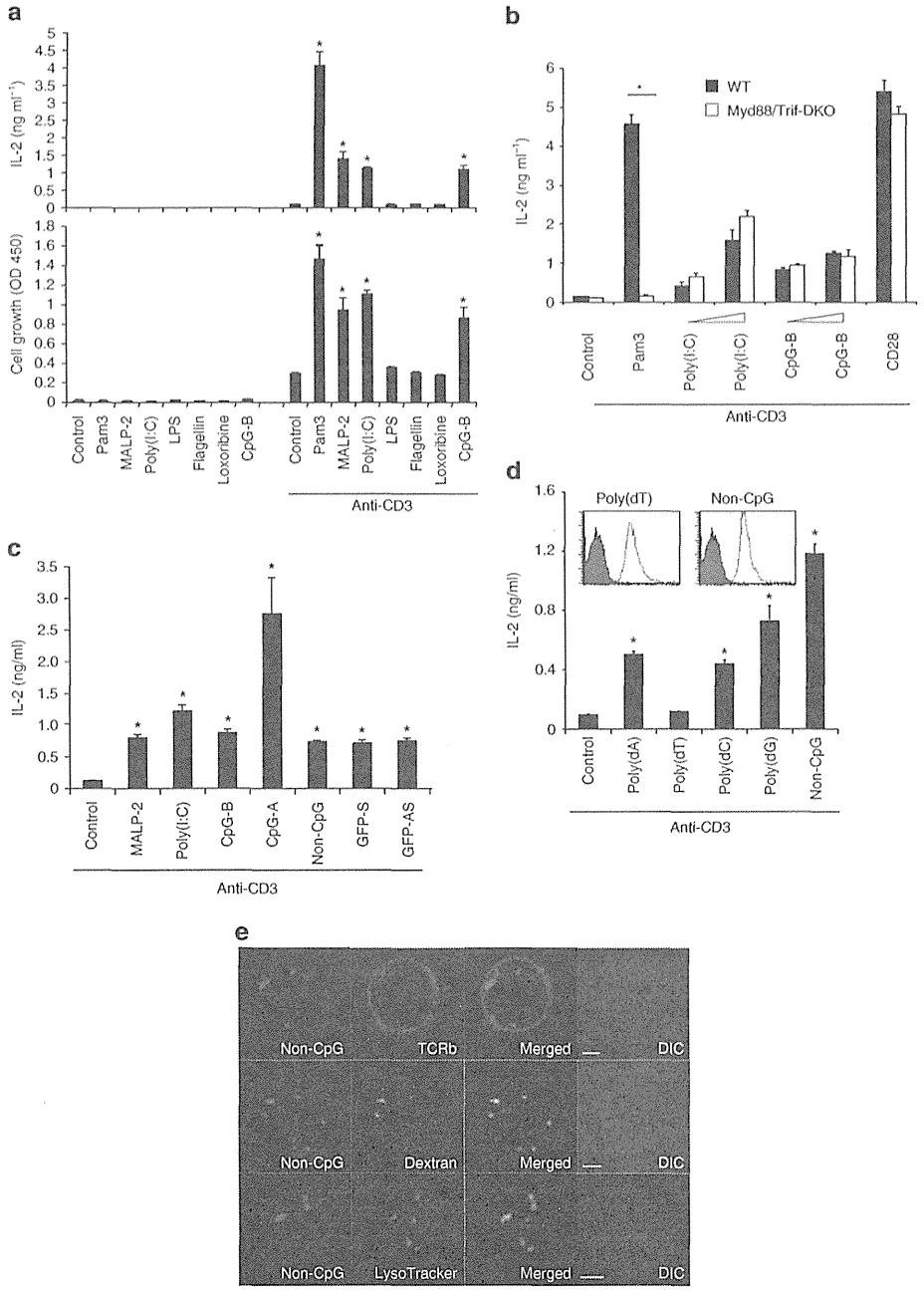

Figure 1 | DNA/RNAs are incorporated into and induce costimulation of CD4$^+$ T cells. (**a**) Naive CD4$^+$ T cells were cultured with indicated TLR ligands (Pam3: 5 μg ml^{-1}, MALP-2: 5 μg ml^{-1}, poly(I:C): 100 μg ml^{-1}, Flagellin: 1 μg ml^{-1}, Loxoribine: 100 μM, CpG-B: 5 μM) in the presence or absence of immobilized anti-CD3ε Ab (10 μg ml^{-1}). After 48-hour incubation, IL-2 production and cell growth were assessed by ELISA and MTS assay, respectively. *$P<0.05$, Student's *t*-test (compared with anti-CD3 alone). (**b**) Naive CD4$^+$ T cells from WT or *Myd88*$^{-/-}$*Trif*$^{-/-}$ mice were stimulated with the indicated TLR ligands or anti-CD28 (Clone: 37.51, 5 μg ml^{-1}) in the presence of immobilized anti-CD3ε Ab. *$P<0.05$, Student's *t*-test (compared with WT cells treated with Pam3). (**c**,**d**) Naive CD4$^+$ T cells were stimulated with the indicated NAs (**c**) and ODNs (**d**) in the presence of immobilized anti-CD3ε Ab. These T cells were incubated with the Cy5-labelled ODNs at 37 °C for 90 min and ODN uptake was determined by flow cytometry (**d**, upper). *$P<0.05$, Student's *t*-test (compared with anti-CD3 alone). (**e**) Naive CD4$^+$ T cells were incubated with 5 μM non-CpG-Cy5 for 90 min and dextran-Alexa Fluor 488 or LysoTracker for last 10 min for the subcellular staining of endosomes and lysosomes, respectively. Confocal microscopy data with differential interference contrast (DIC) images of representative cells are shown. Scale bars, 2.5 μm. Error bars indicate s.d. Data are representative of at least three independent experiments.

It has been reported that poly(I) forms parallel four-stranded helices held together by hydrogen-bonded inosine quartets, similar to poly(dG) chains[18]. We found that heat denaturation of poly(I:C) and poly(G) resulted in impaired costimulation (Fig. 2g), indicating that the ability of RNA to induce T-cell costimulation is dependent on the higher-order structure similar to DNA.

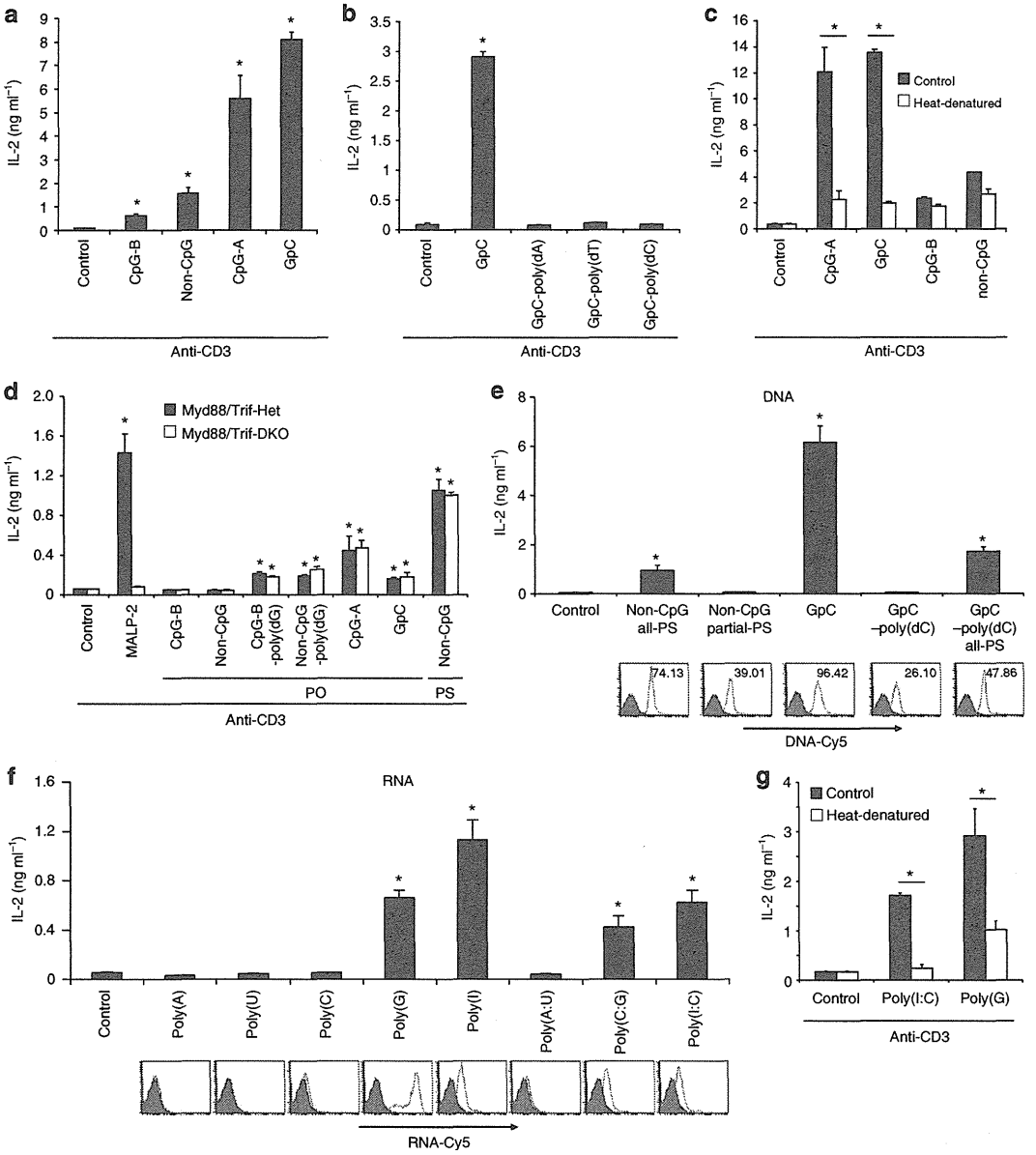

Figure 2 | Properties of DNA/RNAs required for T cell costimulatory activity. (**a**–**c**) Naive CD4$^+$ T cells were activated with plate-bound anti-CD3ε with various DNAs—*$P<0.05$, Student's *t*-test (compared with anti-CD3 alone) (**a**); GpC with different poly tails. *$P<0.05$, Student's *t*-test (compared with anti-CD3 alone) (**b**); and heat-denatured ODNs. *$P<0.01$, Student's *t*-test (compared with the untreated control) (**c**). After 48 h, IL-2 production was measured by ELISA. (**d**) Naive CD4$^+$ T cells derived from *Myd88*$^{+/-}$ *Trif*$^{+/-}$ and *Myd88*$^{-/-}$ *Trif*$^{-/-}$ mice were activated with immobilized anti-CD3ε together with the indicated DNAs. *$P<0.05$, Student's *t*-test (compared with anti-CD3 alone in WT cells). (**e**) Naive CD4$^+$ T cells were stimulated with immobilized anti-CD3ε together with all (all-PS) or partially (partial-PS) PS-modified ODN. CD4$^+$ T cells were incubated with the Cy5-labelled ODN at 37 °C for 90 min, washed and analysed for incorporated ODN by flow cytometry (bottom panels). *$P<0.05$, Student's *t*-test (compared with anti-CD3 alone). (**f**) Naive CD4$^+$ T cells were stimulated with indicated ODNs and analysed similarly as in (**e**). *$P<0.05$, Student's *t*-test (compared with anti-CD3 alone). (**g**) Naive CD4$^+$ T cells were stimulated and analysed similarly in (**c**). *$P<0.05$, Student's *t*-test (compared with the untreated control). Error bars indicate s.d. Data are representative of at least three independent experiments.

Costimulation induced by NA complexed with LL37 and histones. It has been recently shown that endogenous self-DNAs stimulate plasmacytoid dendritic cells by forming aggregated structures upon binding with the antimicrobial peptide LL37 (ref. 19). Similarly, we found that mammalian and bacterial genomic DNA were taken up by T cells and induced costimulation when mixed with LL37 while they alone were neither incorporated nor induce stimulation (Supplementary Fig. 2a, Fig. 3a). Similarly, although poly(A) and poly(A:U) *per se* were defective in cellular uptake and induction of costimulation of naive CD4$^+$ T cells (Fig. 2f), they were incorporated and induced T-cell costimulation when complexed with LL37 (Supplementary Fig. 2b, Fig. 3b).

Similar to LL37, extracellular histones as components of neutrophil extracellular traps exhibit antimicrobial function[20]. We found that the addition of core histones (H2A, H2B, H3 and

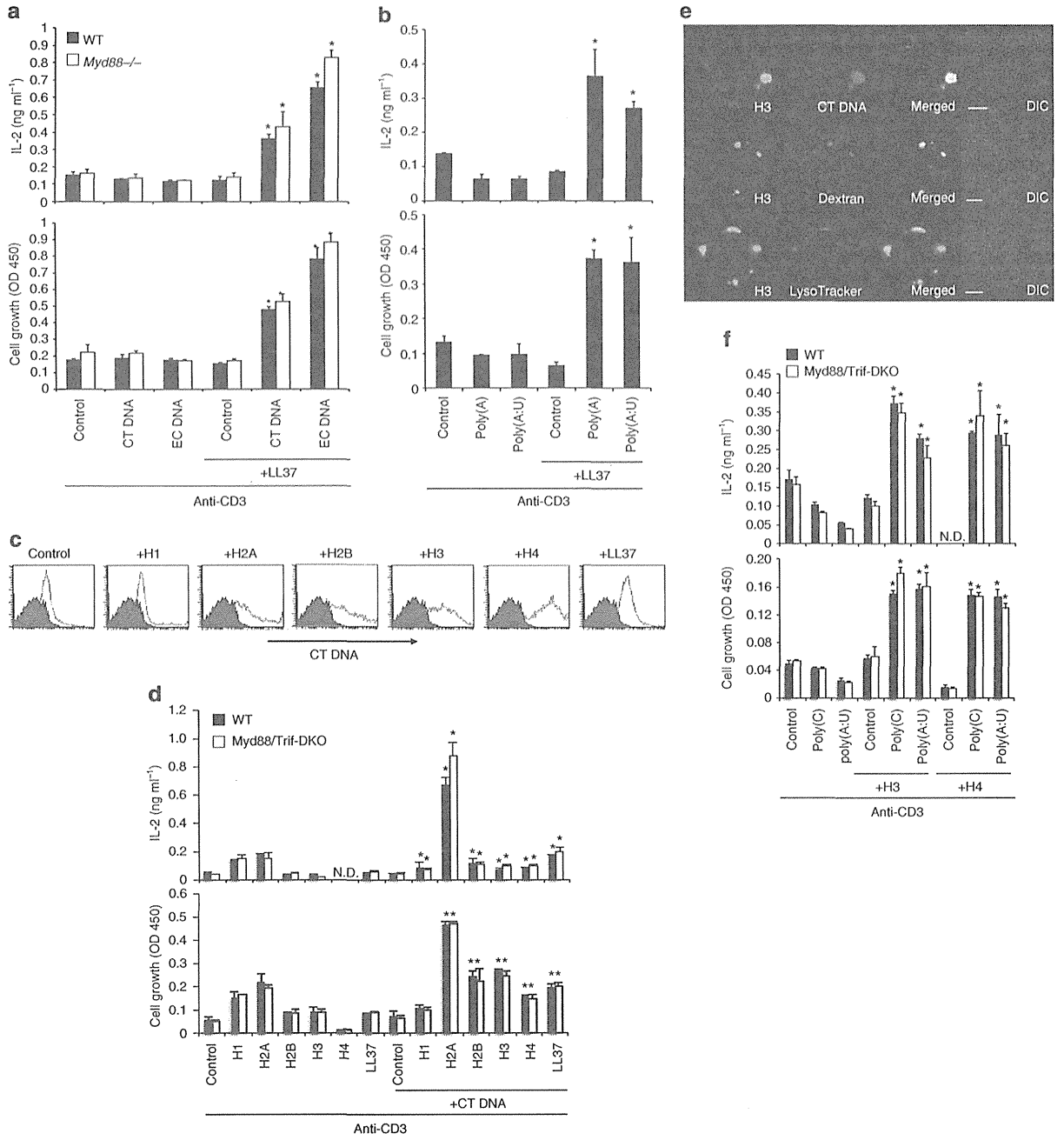

Figure 3 | T-cell activation by NAs complexed with antimicrobial peptides or core histones. (**a**,**b**) Naive CD4$^+$ T cells derived from WT and *Myd88*$^{-/-}$ mice were stimulated with plate-bound anti-CD3ε together with calf thymus (CT)- or *E. coli* (EC)-derived genomic DNA (**a**) or RNAs (**b**) either alone or premixed with LL37. After 48 h, IL-2 production and cell growth were assessed by ELISA and MTS assay, respectively. *$P<0.05$, Student's *t*-test (compared with anti-CD3 plus LL37 in WT cells). (**c**) Naive CD4$^+$ T cells were incubated with the Cy5-labelled CT DNA premixed with the indicated histones or LL37 at 37 °C for 90 min and the incorporated DNA were analysed by flow cytometry. (**d**,**f**) Naive CD4$^+$ T cells derived from WT and *Myd88*$^{-/-}$ *Trif*$^{-/-}$ mice were stimulated with plate-bound anti-CD3 together with CT DNA alone (**d**), RNAs alone (**f**) or premixed with various histones (**d**,**f**), and analysed similarly in (**a**). *$P<0.05$, Student's *t*-test (compared with anti-CD3 plus each histone or LL37 in WT cells). (**e**) Naive CD4$^+$ T cells were stimulated with anti-CD3 with Cy5-labelled CT DNA premixed with Alexa488-labelled histone H3 for 18 h. Endosomes and Lysosomes were visualized by staining with dextran-Alexa Fluor 488 and LysoTracker, respectively. Confocal and differential interference contrast (DIC) images of representative cells are shown. Scale bars, 2.5 μm. Error bars indicate s.d. Data are representative of at least two independent experiments.

H4), but not the linker histone H1, increase cellular uptake of genomic DNA into CD4$^+$ T cells (Fig. 3c). The uptake was correlated with induction of costimulation (Fig. 3d). Although the genomic DNA–H2A complex was the strongest inducer for IL-2 production, H2A itself induces costimulation in the absence of DNA through unknown mechanism. Therefore, we use H3 that has no costimulatory activity by itself to determine the localization of histone/DNA complexes. The genomic

DNA–histone H3 complex was incorporated and localized in endosomes and lysosomes as shown by colocalization with dextran and LysoTracker, respectively (Fig. 3e). Similarly to LL37, histone H3 and H4 allowed poly(C) and poly(A:U) to induce costimulation of naive CD4$^+$ T cells (Fig. 3f). These data indicated that NAs from self or pathogens could induce T-cell costimulation by forming complexes with antimicrobial peptides such as LL37 or core histones.

NA-mediated costimulation is independent of known sensors. To determine the mechanism of NA recognition and activation in T cells, we analysed the possible involvement of cytosolic sensors of NAs in innate cells. DNA-dependent activator of IRFs (DAI; also known as ZBP1) was first reported to function as a cytoplasmic DNA receptor[21]. Absent in melanoma 2 (AIM2) was identified as a cytosolic DNA sensor that activates inflammasome[22]. Stimulator of IFN genes (STING) and TBK1 have been identified as essential molecules that mediate a wide range of cytosolic DNA-induced type I IFN responses[23–25]. To examine the possible involvement of these sensors for T-cell costimulation, we tested naive CD4$^+$ T cells derived from *Zbp1*$^{-/-}$, *Asc*$^{-/-}$ (which links AIM2 to caspase-1), *Sting*$^{-/-}$ and *Tnf*$^{-/-}$ *Tbk1*$^{-/-}$ mice. However, surprisingly, DNA-mediated costimulation was induced normally in these T cells (Fig. 4a–c, Supplementary Fig. 3a), strongly suggesting that T cells utilize a DNA-sensing system different from innate immune cells.

TLR3 recognizes poly(I:C) in the endosome and initiates signalling through the adaptor, TRIF[1]. On the other hand, retinoic acid-inducible gene I (RIG-I) and melanoma differentiation-associated gene 5 (MDA5) sense poly(I:C) and viral RNA in the cytoplasm, which activates an adaptor, IFN-β promoter stimulator 1 (IPS-1; also known as MAVS)[26,27]. To examine the possibility that RIG-I/MDA5 and TLR3 may recognize RNA cooperatively or separately in T cells, we examined RNA-mediated T cell costimulation in IPS-1/TRIF-doubly deficient mice. Normal costimulation by poly(I:C) and poly(I) was observed in *Ips-1*$^{-/-}$ *Trif*$^{-/-}$ T cells (Fig. 4d). In addition, to determine the functional redundancy between TLRs and inflammasomes or RIG-I-like receptors (RLRs), we generated MyD88/ASC-and MyD88/IPS-1 doubly-deficient mice. NA-mediated costimulation was normally induced in naive CD4$^+$ T cells from both mutant mice (Supplementary Fig. 3b,c). It has been demonstrated that NAs are promiscuously sensed by HMGB proteins to induce type I IFN and pro-inflammatory cytokines[28]. However, downmodulation of all three HMGB proteins in CD4$^+$ T cells using small interfering RNA did not alter IL-2 production in response to NAs (Supplementary Fig. 3d).

To identify the mechanism underlying the NA-mediated costimulatory signal to induce IL-2 production in T cells, we

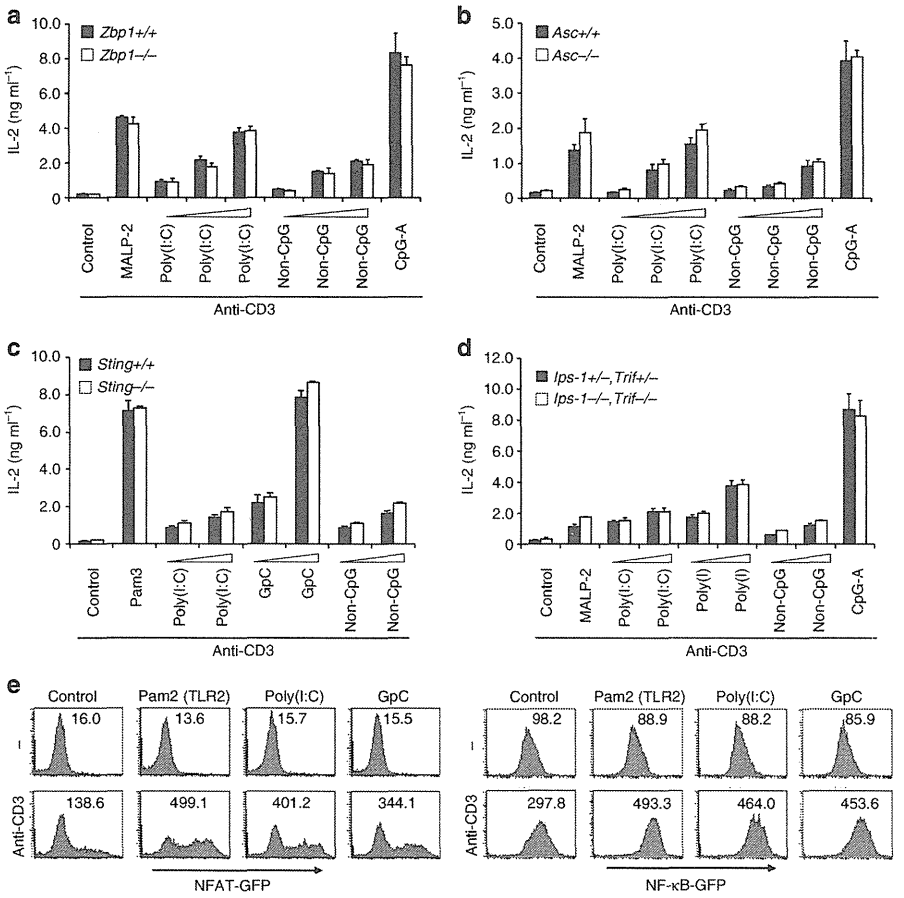

Figure 4 | NA-mediated T cell costimulation is independent of known innate sensors. (**a**–**d**) Naive CD4$^+$ T cells derived from WT or *Zbp1*$^{-/-}$ (**a**), *Asc*$^{-/-}$ (**b**), *Sting*$^{-/-}$ (**c**) or *Ips-1*$^{-/-}$ *Trif*$^{-/-}$ (**d**) mice were stimulated with plate-bound anti-CD3ε and the indicated ligands. After 48 h, IL-2 production was measured by ELISA. (**e**) T-cell hybridoma reporter cells expressing NFAT-GFP (left) or NF-κB-GFP (right) were stimulated with the indicated ligands with or without immobilized anti-CD3ε for 24 h and analysed by flow cytometry. Error bars indicate s.d. Data are representative of at least two independent experiments.

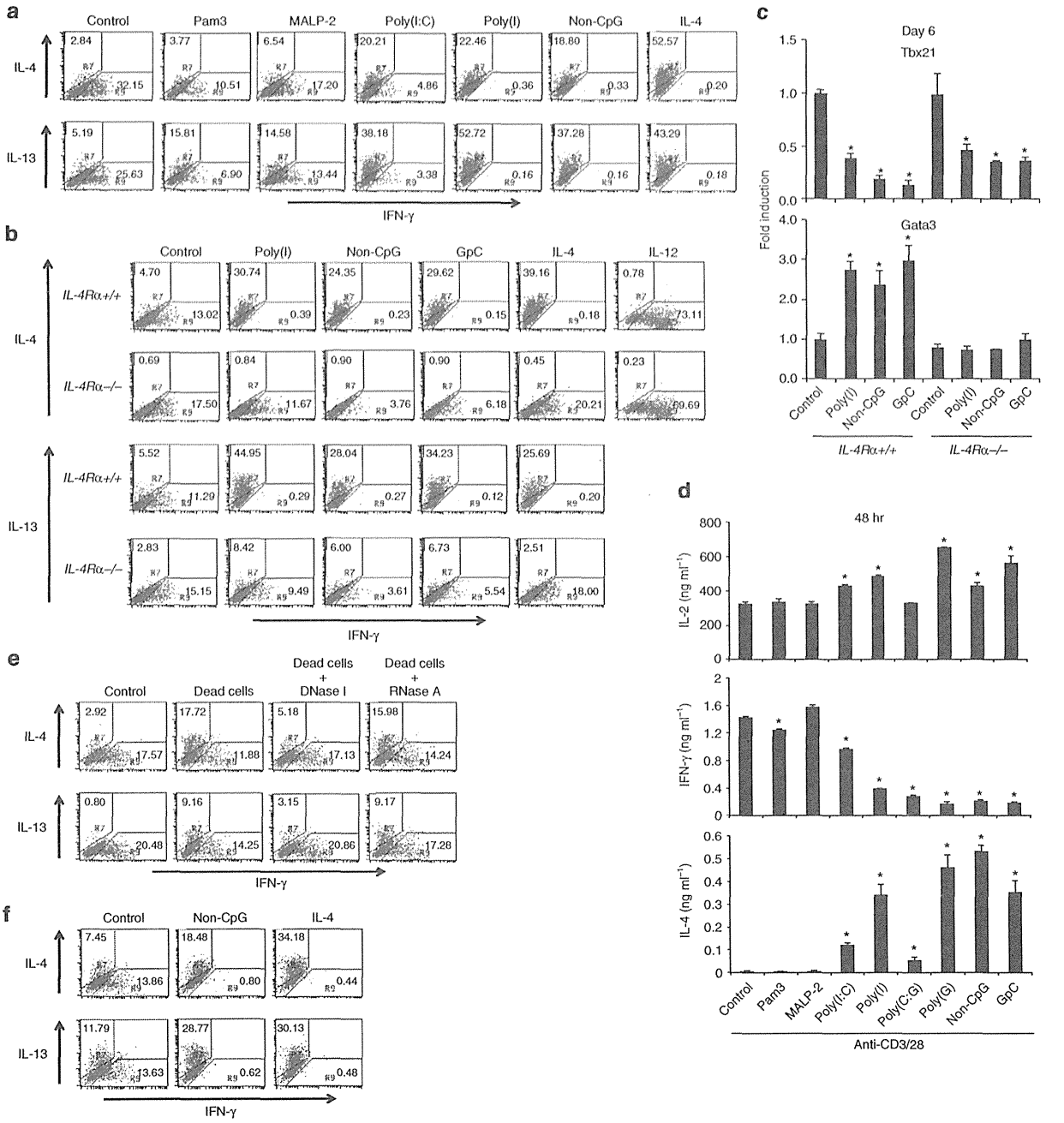

Figure 5 | NA-mediated costimulation induces Th2 differentiation. (**a**) Naive CD4$^+$ T cells were stimulated with immobilized anti-CD3ε (10 μg ml^{-1}) plus anti-CD28 (10 μg ml^{-1}) and the indicated ligands for 3 days, followed by culture with IL-2 (10 ng ml^{-1}) for an additional 3 days. Cells were subjected to real-time PCR analysis (**b**), or restimulated with immobilized anti-CD3ε plus anti-CD28 for 6 h for staining of intracellular cytokines IL-4 and IL-13. (**b**,**c**) Naive CD4$^+$ T cells from WT and IL-4Rα$^{-/-}$ mice were activated similarly as in (**a**) and cells were subjected to real-time PCR analysis (**c**) or restimulated with immobilized anti-CD3ε plus anti-CD28 for 6 h for staining of intracellular cytokines IL-4 and IL-13. *$P<0.05$, Student's *t*-test (compared with anti-CD3/CD28 plus non-CpG in WT cells). (**d**) Naive CD4$^+$ T cells were stimulated for 48 h with anti-CD3ε plus anti-CD28 and the indicated ligands and cytokine production was analysed by ELISA. *$P<0.05$, Student's *t*-test (compared with anti-CD3/CD28 alone). (**e**) Naive CD4$^+$ T cells with or without γ-irradiated naive CD4$^+$ T cells (Dead cells) at a 1:1 ratio were stimulated with anti-CD3ε plus anti-CD28 in the presence or absence of DNase I or RNase A, and analysed similarly as in (**a**). (**f**) Naive CD4$^+$ T cells from OT-II Tg mice were co-cultured with irradiated T cell-depleted splenocytes from C57BL/6 mice as APCs, together with OVA peptide (10 μM) in the presence or absence of non-CpG for 6 days. CD4$^+$ T cells were restimulated with immobilized anti-CD3ε plus anti-CD28 for 6 h for staining of intracellular cytokines. Error bars indicate s.d. Data are representative of at least three independent experiments.

analysed the activation of NF-κB and NFAT, both of which are essential for T-cell activation[29]. T-cell hybridoma (2B4) expressing the NF-κB-GFP or NFAT-GFP was stimulated by NAs plus anti-CD3. We observed that poly(I:C) and GpC markedly increased activation of NF-κB and NFAT, compared with anti-CD3 alone (Fig. 4e). These data suggest that enhanced

activation of NF-κB and NFAT is involved in the induction of NA-mediated T-cell costimulation. It is also worth noting that NA-induced costimulation of a T-cell hybridoma, which is definitely free of any innate cells, confirms that NA directly stimulates T cells.

NA-mediated costimulation induces Th2 cell differentiation. A recent study demonstrated that DNA released from dying host cells stimulates Th2 responses *in vivo*[30]. It is also reported that stimulation of RLRs by specific ligands biases the immune system toward a Th2 response, whereas the TLR signalling strongly induces Th1 and Th17 responses[31]. Accordingly, it seemed possible that NA-induced stimulation of T cells would induce Th2 cell differentiation. To test this hypothesis, naive $CD4^+$ T cells were stimulated *in vitro* with anti-CD3 plus anti-CD28 together with various NAs without blocking Abs against IFN-γ or IL-4. NAs such as poly(I:C), poly(I) and non-CpG strongly induced the differentiation of IL-4-producing T cells without the addition of exogenous IL-4 (Fig. 5a). By contrast, NAs strongly inhibited the differentiation of IFN-γ-producing T cells (Fig. 5a), and also increased the frequency of Th2 cells producing IL-5, IL-9, IL-13 and IL-10 (Fig. 5a, Supplementary Fig. 4a). Consistently, the expression of the Th2-master regulator GATA-3 was enhanced, whereas the expression of T-bet, the Th1-master regulator was strongly inhibited in the T cells cultured with NAs (Supplementary Fig. 4b), suggesting that NAs directly induce the differentiation of Th2 cells. Notably, unlike NAs, TLR2 ligands had a minimal effect on Th1 and Th2 differentiation (Fig. 5a), and NA-mediated costimulation did not affect the development of IL-17-producing T cells (Supplementary Fig. 4c). Since NAs induced Th2 differentiation of MyD88/TRIF-double deficient T cells similarly to control T cells (Supplementary Fig. 4d), this processes does not require TLR signalling.

The generation of Th2 cells is dependent on IL-4–STAT6 signalling, which leads to the upregulation of GATA-3 (ref. 32). We assessed whether Th2 differentiation induced by NA-mediated costimulation was also IL-4–STAT6-dependent. IL-4 receptor (R) α-deficient T cells after activation by NAs for 6 days failed to produce any Th2 cytokines including IL-4 and IL-13 (Fig. 5b). In addition, the induction of GATA-3 expression was severely diminished in IL-4Rα-deficient T cells (Fig. 5c). Similar results were obtained using *Stat6*$^{-/-}$ $CD4^+$ T cells (Supplementary Fig. 4e), indicating that NA-mediated Th2 differentiation requires IL-4–STAT6 signalling. However, NA-mediated inhibition of IFN-γ production and T-bet expression was still observed in IL-4Rα-deficient T cells (Fig. 5b,c), suggesting that NA-mediated inhibition of Th1 differentiation is independent of IL-4 signalling. Therefore, it is likely that NA-mediated costimulation may enhance IL-4 production at an early time point (within 48 h), which then induces Th2 differentiation. Indeed, IL-4 production was induced at 48 h by NAs but not TLR2 ligands, whereas IFN-γ production was reduced (Fig. 5d). NA-induced enhancement of IL-2 production was not strong upon stimulation with anti-CD3 plus CD28 as compared with anti-CD3 alone. Strong costimulation with anti-CD28 resulted in reduced enhancement, though significantly enhanced (Fig. 5d).

Collectively, these data demonstrate that NAs induce Th2 differentiation in an IL-4 signal-dependent manner similarly to the canonical Th2 differentiation pathway induced by exogenous IL-4, whereas suppression of Th1 differentiation by NAs is independent of IL-4 signalling.

We next determined whether self-DNA from dead cells induce Th2 differentiation. We found that the addition of dead cells (irradiated naive $CD4^+$ T cells or irradiated HEK 293 cells) to the T-cell culture enhanced the differentiation of IL-4-producing cells, which was cancelled by the addition of DNase I into the medium (Fig. 5e, Supplementary Fig. 5f). Addition of RNase A resulted in minimal effect. These data suggest that self-DNA is a critical factor for Th2 differentiation induced by dead cells. To examine whether NA-mediated Th2 differentiation is induced upon antigen stimulation, OVA-specific naive $CD4+$ T cells from OT-II Tg mice were stimulated with OVA peptide-pulsed irradiated splenocytes plus non-CpG. Non-CpG promoted Th2 differentiation under the condition, strongly suggesting that NAs induces T-cell costimulation even when T cells are activated by antigen-pulsed APCs (Fig. 5f).

Mechanisms underlying NA-induced Th2 differentiation. To determine the mechanism by which NAs induces Th2 differentiation, we compared the gene expression profiles in $CD4^+$ T cells activated under neutral conditions in the presence or absence of non-CpG. Surprisingly, before the upregulation of GATA-3, the expression of T-bet was strongly inhibited by non-CpG-mediated costimulation (Fig. 6a). Following the suppression of T-bet expression, the expression of Th2-associated genes was upregulated and IFN-γ was downregulated at 48 h after stimulation (Fig. 6a). We further confirmed that various NAs other than non-CpG also induced the suppression of T-bet and the upregulation of GATA-3 and IL-4 expression (Supplementary Fig. 5a). We then compared the kinetics of the expression of Th1/Th2-associated genes upon stimulation with IL-4 or non-CpG. GATA-3 was quickly induced in $CD4^+$ T cells by exogenous IL-4 (at 24 h), followed by the induction of Th2 cytokines and the inhibition of T-bet and IFN-γ expression. By contrast, in $CD4^+$ T cells stimulated with non-CpG, GATA-3 expression was induced after inhibition of T-bet expression, suggesting that Th2-associated genes are indirectly induced by non-CpG-mediated costimulation. In addition to these kinetic differences, inhibition of T-bet expression by non-CpG was more rapid and robust than by exogenous IL-4 (Fig. 6b). T-bet inhibits Th2 differentiation by directly inhibiting the expression of Th2 cytokines and sequestering GATA-3 from the promoters of Th2 cytokines[33]. Using ChIP analysis, we showed that the binding of GATA-3 to the IL-4 and IL-13 promoters was enhanced in $CD4^+$ T cells by stimulation with non-CpG (Fig. 6c). Therefore, it is likely that NA-mediated costimulation induces Th2 differentiation primarily by inhibiting T-bet expression.

To test this hypothesis further, we compared Th2 differentiation by the blockade of IFN-γ signalling and non-CpG stimulation, because the expression of T-bet is controlled by IFN-γ signalling[34]. We found that the T-bet expression in $CD4^+$ T cells cultured in the presence of anti-IFN-γ was much lower than those stimulated with non-CpG at early time point (48 h) after TCR stimulation (Fig. 6d). However, the expression of GATA-3 and Th2 cytokines in T cells cultured with anti-IFN-γ was much lower than those stimulated with non-CpG (Fig. 6d), suggesting that inhibition of T-bet expression by non-CpG is not sufficient, though partially contributes, for the upregulation of Th2-associated gene expression. Additional signal(s) are required for the induction of Th2-associated genes by non-CpG-mediated costimulation. Consistently, the Th2 polarization by the presence of anti-IFN-γ was weaker than by non-CpG later (day 6) after TCR priming (Fig. 6e). Thus, non-CpG-mediated costimulation simultaneously inhibits T-bet expression and enhances the expression of Th2-associated genes.

As T-bet controls Th1 development by directly activating IFN-γ (ref. 34), it is likely that NA-mediated costimulation would inhibit Th1 development under Th1-polarizing conditions. As expected, non-CpG inhibits Th1 development and

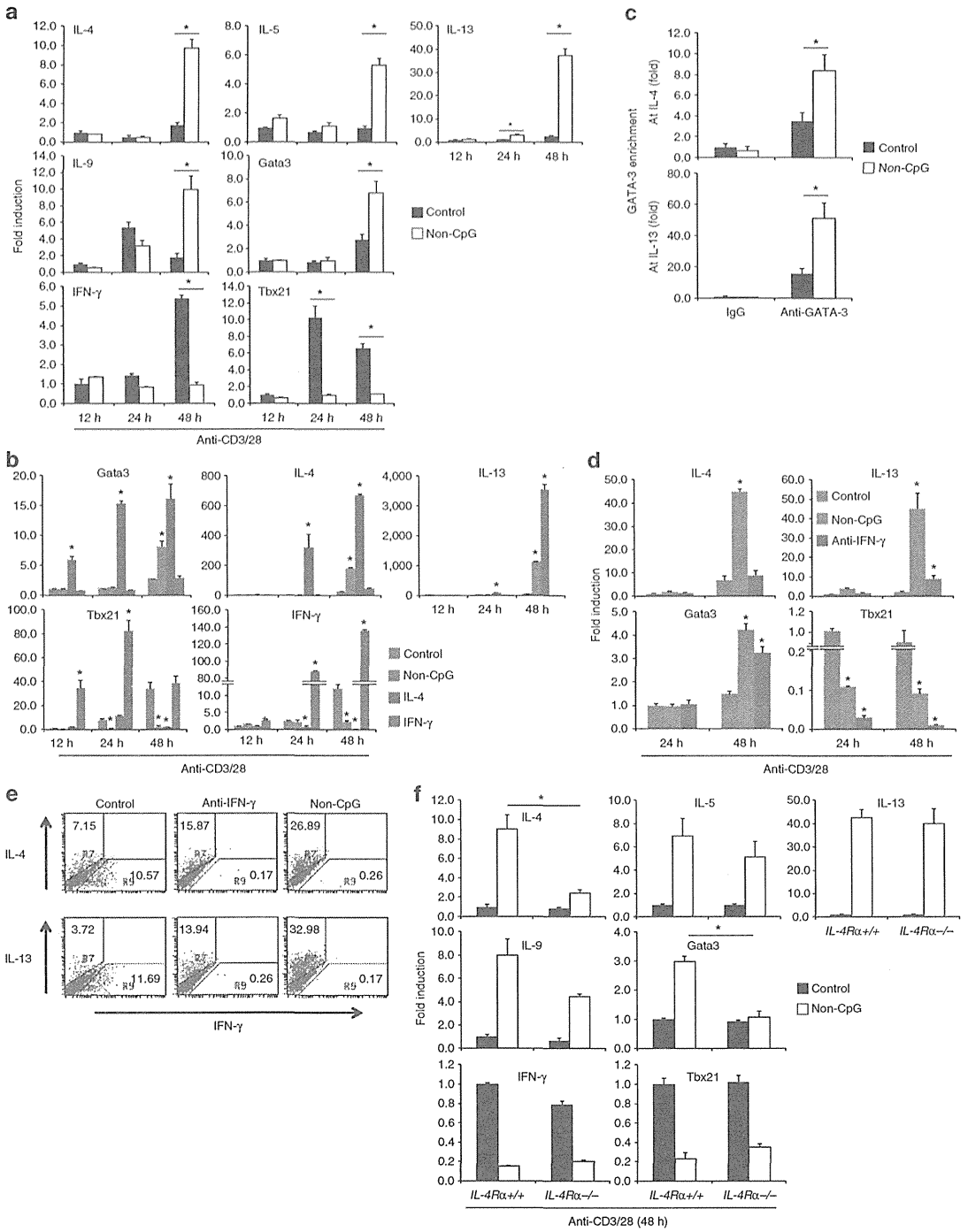

Figure 6 | Molecular mechanism of NA-mediated Th2 differentiation. (**a**) Naive CD4$^+$ T cells were stimulated with anti-CD3ε plus anti-CD28 with or without non-CpG for the indicated periods and mRNA expression was analysed by real-time PCR. *$P<0.01$, Student's *t*-test (compared with anti-CD3/CD28 alone). (**b**) Naive CD4$^+$ T cells were stimulated by NAs or IL-4 and analysed similarly in (**a**). *$P<0.01$, Student's *t*-test (compared with anti-CD3/CD28 alone). (**c**) Naive CD4$^+$ T cells were stimulated with anti-CD3ε plus anti-CD28 together with non-CpG for 48 h, and ChIP analyses were performed by immunoprecipitation with control Ab (IgG) or anti-GATA-3. Quantitative PCR analysis of the GATA3 binding at the IL-4 and IL-13 gene promoters. The results were normalized to those of a standardized aliquot of input chromatin. *$P<0.05$, Student's *t*-test (compared with anti-CD3/CD28 alone). (**d**,**e**) Naive CD4$^+$ T cells were stimulated in the presence of non-CpG or anti-IFN-γ Ab and mRNA expression (**d**) and intracellular cytokine expression (day 6) (**e**) were analysed. *$P<0.01$, Student's *t*-test (compared with anti-CD3/CD28 alone). (**f**) Naive CD4$^+$ T cells from WT and IL-4Rα$^{-/-}$ mice were stimulated and analysed similarly in (**a**). *$P<0.01$, Student's *t*-test (compared with anti-CD3/CD28 plus non-CpG in WT cells). Error bars indicate s.d. Data are representative of at least two independent experiments.

IFN-γ production even under Th1 differentiation condition (Supplementary Fig. 5b).

We then analysed whether IL-4 signalling is required for the early expression of Th2-associated genes after NA-mediated costimulation. Interestingly, the augmentation of the expression of IL-4 and GATA-3 by non-CpG was severely impaired in IL-4Rα-deficient $CD4^+$ T cells, whereas the upregulation of IL-5, IL-9 and IL-13 expression and downregulation of IFN-γ and T-bet expression was largely unaffected (Fig. 6f). Similar results were obtained in the *Stat6*$^{-/-}$ $CD4^+$ T cells (Supplementary Fig. 5c). These data suggest that non-CpG-mediated T-cell costimulation directly induced the expression of IL-5, IL-9 and IL-13, partly through the inhibition of T-bet expression, whereas IL-4 and GATA-3 expression was induced by IL-4–STAT6 signalling. Naive $CD4^+$ T cells are capable of producing IL-4 upon primary TCR stimulation in the absence of exogenous IL-4, and the early IL-4 is rapidly consumed by the $CD4^+$ T cells themselves[35]. Therefore, NA-mediated IL-4 production may require early IL-4 autocrine signalling to induce the autoactivation of GATA-3 expression. Notably, however, expression of all Th2-associated genes in IL-4Rα-deficient $CD4^+$ T cells disappeared by day 6 after priming with NAs. Although non-CpG stimulation induces the enrichment of GATA-3 on the IL-13 promoter (Fig. 6c), it seems that early induction of IL-13 expression by non-CpG (at 48 h) is independent of GATA-3 because IL-13 expression was enhanced by non-CpG in IL-4Rα-deficient $CD4^+$ T cells despite the lack of GATA-3 upregulation by non-CpG (Fig. 6f). However, it seems that the enrichment of GATA-3 on the IL-13 promoter is critical for IL-13 expression later (in day 6) after TCR priming for its maintenance because the induction of IL-13 and GATA-3 expression by non-CpG was diminished later after TCR priming (in day 6) in IL-4Rα-deficient $CD4^+$ T cells (Fig. 5b,c). These data indicate that autocrine IL-4 is required for the induction of IL-4 and GATA-3 upon non-CpG stimulation, which then acts to amplify and stabilize the expression of Th2-associated genes.

Discussion

The present study shows that NAs directly stimulate $CD4^+$ T cells through a NA sensor different from those of the innate system, subsequently leading to Th2 cell differentiation. In addition to TLRs, a growing number of NA sensors have been identified in the innate immune system, including RLRs, IPS-1-dependent sensors, MyD88/TRIF-dependent sensors, ASC-dependent inflammasomes and STING-dependent sensors[36]. However, we found that recognition of NAs by T cells is independent of all of these known sensors including HMGBs, although we cannot conclusively exclude the possibility that some known NA sensors work redundantly.

We found that a higher-order structure of the NAs is required for their incorporation by T cells. Since T cells can incorporate genomic self-DNA only when it is complexed with antimicrobial peptides or core histones, T cells may respond to NAs from dying cells at the site of inflammation and infection, where antimicrobial peptides and/or histones are released. We also demonstrated that specific recognition and uptake of RNA induces costimulatory responses. A recent study demonstrated that cells infected with several viruses including vaccinia virus contained higher-order structured RNA that stimulated MDA5 (ref. 37), indicating the possibility that T cells may recognize such viral RNA and are activated. Recent studies demonstrated that, upon infection with nonpermissive HIV, cytoplasmic DNA derived from incomplete reverse transcripts caused $CD4^+$ T cell death through recognition of the cytosolic DNA by a sensor IFI16 followed by activation of the ASC-caspase-1 pathway[38,39]. It was also reported that transfected DNA was colocalized with IFI16 in activated T cells[40]. However, our result that DNA-mediated costimulation was normally induced in ASC-deficient $CD4^+$ T cells suggests that IFI16 is not involved in the DNA-mediated costimulation in T cells. While cytosolic DNA stimulates IFI16 upon HIV infection or DNA transfection, incorporated DNAs are accumulated in endosome/lysosome and induce T-cell costimulation in our experiments without activation of IFI16 probably due to the failure to deliver DNA to the cytosol.

Furthermore, a recent study showed that immunization with RLR ligands or infection with viruses, which mainly activate RLRs, results in enhanced Th2 responses and much weaker Th1 responses[31], supporting our observation that NAs directly stimulate the induction of Th2 responses. It is known that TLR stimulation of innate immune cells promotes Th1 and Th17 responses by inducing the Th1-polarizing cytokine IL-12 and the Th17-polarizing cytokines IL-6/IL-23/IL-1 (refs 1,41). Recent studies, including ours, show that TLR2 ligands directly activate Th1 but not Th2 cells[7] and promote Th17 differentiation[8]. In contrast to TLR, the activation of RLRs suppresses Th1 and Th17 differentiation through the inhibition of IL-12 and IL-23 production, resulting in the enhanced differentiation of Th2 cells[31]. Our results demonstrate that direct stimulation of T cells by NAs strongly inhibit the initial expression of T-bet, which allows the initial production of IL-4 and Th2 cytokines to induce Th2 differentiation. Thus, similar to Th1 and Th17 responses induced by TLRs in innate cells and T cells, it is likely that activation of RLRs in innate cells and the NA sensor in T cells by NAs cooperatively induces Th2 differentiation.

The initial origin of IL-4 to trigger Th2 differentiation has been extensively analysed but remains unclear. It has been reported that basophils serve as Th2 cell-promoting APCs by producing IL-4 and/or thymic stromal lymphopoietin[14]. However, their role as APCs remains controversial[42]. It has been suggested that naive T cells are a possible source of IL-4 (refs 43,44), which modestly induces Th2 differentiation when IFN-γ and IL-12 are neutralized[35]. Although it has been proposed that Th2 differentiation may occur as a default pathway, $CD4^+$ T cells in IL-12 p40-deficient mice fail to differentiate into Th2 cells in response to intracellular pathogens[45]. Thus, the simple blocking of Th1-inducing stimuli such as IL-12 or IFN-γ is not sufficient to induce Th2 differentiation, suggesting the existence of additional Th2-inducing factors. However, such factors for the initial triggering of IL-4 production from naive $CD4^+$ T cells under physiological conditions have not been identified. We here provide strong evidence that the initial IL-4 production derived from naive $CD4^+$ T cells upon recognition of NAs in the absence of any exogenous cytokines or neutralizing antibodies instructs naive $CD4^+$ T cells to differentiate into Th2 cells.

A recent report demonstrated that aluminium hydroxide adjuvant (alum) causes cell death and release of host DNA at sites of immunization, which mediates the adjuvant effect for Th2-biased adaptive responses[30]. As the mechanism to induce Th2 responses, it has been reported that uric acid released in the peritoneal cavity after injection of alum may have a role in promoting Th2 cell responses independently of the ASC inflammasome or TLR signalling[46]. As uric acid crystals released at the sites of immunization/inflammation induce extracellular DNA traps formation by neutrophil, eosinophil and basophil[47], uric acid-induced extracellular DNA traps may directly stimulate T cells to induce Th2 response. A recent study reported that defects in clearance of apoptotic airway epithelial cells upon environmental allergen encounter lead to augmented Th2 cytokine production and airway hyper-responsiveness[48], indicating that *in vivo* Th2 responses are closely related to host

cell death accompanied by host DNA release. In line with the hypothesis, we found that self-DNA from dead cells induces Th2 differentiation.

Collectively, we have identified NAs as a direct Th2-inducing factor, which induces initial production of IL-4 by naive $CD4^+$ T cells, which in turn induces Th2 differentiation. Although we have not identified the NAs sensor in T cells yet, our results provide the possibility that NAs may be critical targets for the development of improved vaccine adjuvants and the overall design of therapeutics to control allergic diseases.

Methods

Mice. C57BL/6 mice were purchased from Clea Japan, Inc. The mice deficient in MyD88, TRIF-deficient, IPS-1 ZBP1 and STAT6 were provided by Dr Akira S. *Asc*$^{-/-}$ mice were provided by Dr Taniguchi S and Dr Noda T. *Sting*$^{-/-}$ and *Il4ra*$^{-/-}$ mice were provided by Dr Barber GN and Dr Brombacher F, respectively. Mice aged 8–16 weeks were used. All mice were maintained under specific pathogen-free conditions and all experiments were conducted under protocols approved by RIKEN Yokohama Institute.

ELISA and cell growth analysis. Cell culture supernatants were analysed by ELISA for the production of IL-2 (BD biosciences), IL-4 (BD biosciences) and IFN-γ (BD biosciences). Cell growth was assessed by the MTS assay-based Cell Counting Kit-8 (DOJINDO).

Helper T-cell differentiation. $CD4^+$/$CD25^-$/$CD62L^+$/$NK1.1^-$ (naive) T cells were isolated from spleens using a FACS-Aria cell sorter. For Th0 cells, cells were stimulated with plate-bound anti-CD3 (2C11, 10 μg ml^{-1}) and anti-CD28 (PV-1, 10 μg ml^{-1}) Abs in the presence of the indicated ligands. For Th1 cells, cells were cultured in the presence of IL-12 (10 ng ml^{-1}) and anti-IL-4 Abs (10 μg ml^{-1}). For Th2 cells, cells were similarly cultured in the presence of IL-4 (10 ng ml^{-1}).

Real-time quantitative PCR. After removal of genomic DNA by treatment with DNase (Wako Nippon Gene), randomly primed cDNA strands were generated with reverse transcriptase II (Invitrogen). RNA expression was quantified by real-time PCR with the following gene-specific primers and values were normalized to the expression of *Rps18* mRNA (Supplementary Table 2).

Reagents and Abs. The TLR2 ligands *N*-palmitoyl-*S*-(2,3-bis(palmitoyloxy)-(2*RS*)-propyl)-Cys-Ser-Lys_4 (Pam3) and macrophage-activating lipopeptide 2 (MALP-2) were purchased from EMC Microcollections. Poly(I:C), a TLR3 ligand, and LPS (*Escherichia. coli* O111:B4), a TLR4 ligand, were obtained from GE Healthcare Biosciences and Sigma, respectively. Flagellin, a TLR5 ligand, and loxoribine, a TLR7 ligand, were obtained from InvivoGen. Oligo DNAs including TLR9 ligands were purchased from Hokkaido System Science. Poly(A), poly(U), poly(C), poly(G), poly(I), poly(A:U) and poly(C:G) were purchased from Sigma. Calf thymus DNA and *E. coli* DNA was from Sigma and Invivogen, respectively. LL37 was from AnaSpec. Histone H1, H2A, H2B, H3 and H4 were from New England BioLabs. LL37 or histones were first premixed with genomic DNA (peptide:DNA mass ratio of 2:1). After 30-min incubation at room temperature, the mix was added to the T-cell cultures (final concentration was 10 μg ml^{-1} of DNA).

Abs specific for anti-IL-4 PE (11B11, 1:25 dilution) and anti-IFN-γ FITC (XMG1.2, 1:25 dilution) were obtained from BD Biosciences; anti-IL-5 PE (TRFK5, 1:25 dilution), anti-IL-10 PE (1:25 dilution) and anti-IL-13 PE (eBio13A, 1:25 dilution) from eBioscience; anti-IL-9 PE (RM9A4, 1:25 dilution) from BioLegend. ChIP analysis used mAb to GATA-3 (HG3-31AC; Santa Cruz, 1:125 dilution).

Intracellular cytokine staining analysis. $CD4^+$ T cells were restimulated with immobilized anti-CD3 and anti-CD28 for 6 h in the presence of 2 μM monensin (Sigma, St Louis, MO). Cells were fixed with 4% paraformaldehyde and permeabilized with 0.5% Triton X-100. After blocking with 3% BSA-PBS, cells were stained with antibodies to each cytokine. Flow cytometric analysis was performed on a FACSCalibur and data were analysed with BD CellQuest.

Cellular uptake of NA. To analyse the uptake of NA, 2×10^5 cells were pre-incubated at 37 °C for 10 min in medium. Cells were incubated with fluorescence-labelled NA at 37 °C for 90 min. Then cells were washed once in HANKS/0.1% BSA followed by an acidic wash with 100 mM acetic acid, 150 mM NaCl (pH2.7) for 1 min to remove unbound and cell surface-bound NA. Subsequently, cells were washed two times in HANKS/0.1% BSA, and were analysed by flow cytometry using the FACSCalibur.

Reporter cells. The 2B4–NFAT-GFP cells have been described[49] and the 2B4-NF-kB-GFP cells were established by transfection of NF-κB-GFP into 2B4 hybridoma cells. These cells were cultured in RPMI 1640 medium supplemented with 10% (vol/vol) FCS and β-mercaptoethanol.

Chromatin immunoprecipitation assay. Cells were fixed for 10 min at 4 °C with 10% formaldehyde. After incubation, glycine was added to a final concentration of 0.125 M to quench the formaldehyde. Cells were pelleted, washed three times with ice-cold PBS and then lysed. The lysates were sonicated to reduce DNA length to between 200 and 300 base pairs. The chromatin was pre-cleared with protein G agarose beads for 6 h and then incubated with 4 μg of anti-GATA-3 (HG3-31) agarose conjugate antibody (Santa Cruz, sc-268 AC) or control IgG overnight. The precipitates were washed and eluted in 120 μl of $NaHCO_3$ buffer with 1% SDS. The samples were treated with RNase and Proteinase K and then de-crosslinked at 65 °C overnight. Precipitated DNA was further purified with Qiaquick PCR purification kit (Qiagen) and was analysed by quantitative PCR (Supplementary Table 2)[50].

Confocal microscopic imaging. Cells were settled on glass-bottom, 35-mm tissue culture dishes (MATSUNAMI GLASS). Confocal microscopy analyses were performed with a Leica TCS SP5 confocal microscope with an oil immersion objective (HCX PL APO ×63/1.40–0.60 NA, Leica). Dual-color images were acquired using a sequential acquisition mode to avoid cross-excitation. To visualize the Histone–calf thymus DNA complex in $CD4^+$ T cells, calf thymus DNA (Sigma) was labelled with Cy5 using the Label IT Nucleic Acid Labelling Reagents (Mirus) and histone H3 was labelled with DyLight 488 using the antibody labelling kit (Pierce), according to the standard protocol provided by the respective manufacturers.

RNA interference. Double-stranded oligonucleotides corresponding to the target sequences were cloned into the pSuper.Retro RNAi plasmid (OligoengineInc.). The siRNA targeting sequences which function for commonly all three murine HMGB1/2/3 are 5′-GAGAAGTATGAGAAGGATATT-3′ and 5′-AAGTATGAGA AGGATATTGCT-3′.

Statistics. Statistical significance was determined by a two-tailed unpaired Student's *t*-test. $P<0.05$ was considered statistically significant.

References

1. Takeda, K., Kaisho, T. & Akira, S. Toll-like receptors. *Annu. Rev. Immunol.* **21,** 335–376 (2003).
2. Medzhitov, R. Toll-like receptors and innate immunity.. *Nat. Rev. Immunol.* **1,** 135–145 (2001).
3. Komai-Koma, M., Jones, L., Ogg, G. S., Xu, D. & Liew, F. Y. TLR2 is expressed on activated T cells as a costimulatory receptor. *Proc. Natl Acad. Sci. USA* **101,** 3029–3034 (2004).
4. Cottalorda, A. *et al.* TLR2 engagement on CD8 T cells lowers the threshold for optimal antigen-induced T cell activation. *Eur. J. Immunol.* **36,** 1684–1693 (2006).
5. Sutmuller, R. P. *et al.* Toll-like receptor 2 controls expansion and function of regulatory T cells. *J. Clin. Invest.* **116,** 485–494 (2006).
6. Liu, H., Komai-Koma, M., Xu, D. & Liew, F. Y. Toll-like receptor 2 signaling modulates the functions of CD4+ CD25+ regulatory T cells. *Proc. Natl Acad. Sci. U. S. A.* **103,** 7048–7053 (2006).
7. Imanishi, T. *et al.* Cutting edge: TLR2 directly triggers Th1 effector functions. *J. Immunol.* **178,** 6715–6719 (2007).
8. Reynolds, J. M. *et al.* Toll-like receptor 2 signaling in CD4(+) T lymphocytes promotes T helper 17 responses and regulates the pathogenesis of autoimmune disease. *Immunity* **32,** 692–702 (2010).
9. Caron, G. *et al.* Direct stimulation of human T cells via TLR5 and TLR7/8: flagellin and R-848 up-regulate proliferation and IFN-gamma production by memory CD4+ T cells. *J. Immunol.* **175,** 1551–1557 (2005).
10. Gelman, A. E. *et al.* The adaptor molecule MyD88 activates PI-3 kinase signaling in CD4+ T cells and enables CpG oligodeoxynucleotide-mediated costimulation. *Immunity* **25,** 783–793 (2006).
11. Gelman, A. E., Zhang, J., Choi, Y. & Turka, L. A. Toll-like receptor ligands directly promote activated CD4+ T cell survival. *J. Immunol.* **172,** 6065–6073 (2004).
12. Peng, G. *et al.* Toll-like receptor 8-mediated reversal of CD4+ regulatory T cell function. *Science* **309,** 1380–1384 (2005).
13. Zhu, J., Yamane, H. & Paul, W. E. Differentiation of effector CD4 T cell populations (*). *Annu. Rev. Immunol.* **28,** 445–489 (2010).
14. Paul, W. E. & Zhu, J. How are T(H)2-type immune responses initiated and amplified? *Nat. Rev. Immunol.* **10,** 225–235 (2010).
15. Kerkmann, M. *et al.* Spontaneous formation of nucleic acid-based nanoparticles is responsible for high interferon-alpha induction by CpG-A in plasmacytoid dendritic cells. *J. Biol. Chem.* **280,** 8086–8093 (2005).
16. Bishop, J. S. *et al.* Intramolecular G-quartet motifs confer nuclease resistance to a potent anti-HIV oligonucleotide. *J. Biol. Chem.* **271,** 5698–5703 (1996).

17. Dalpke, A. H., Zimmermann, S., Albrecht, I. & Heeg, K. Phosphodiester CpG oligonucleotides as adjuvants: polyguanosine runs enhance cellular uptake and improve immunostimulative activity of phosphodiester CpG oligonucleotides *in vitro* and *in vivo*. *Immunology* **106,** 102–112 (2002).
18. Arnott, S., Chandrasekaran, R. & Marttila, C. M. Structures for polyinosinic acid and polyguanylic acid. *Biochem. J.* **141,** 537–543 (1974).
19. Lande, R. *et al.* Plasmacytoid dendritic cells sense self-DNA coupled with antimicrobial peptide. *Nature* **449,** 564–569 (2007).
20. Mantovani, A., Cassatella, M. A., Costantini, C. & Jaillon, S. Neutrophils in the activation and regulation of innate and adaptive immunity. *Nat. Rev. Immunol.* **11,** 519–531 (2011).
21. Takaoka, A. *et al.* DAI (DLM-1/ZBP1) is a cytosolic DNA sensor and an activator of innate immune response. *Nature* **448,** 501–505 (2007).
22. Hornung, V. *et al.* AIM2 recognizes cytosolic dsDNA and forms a caspase-1-activating inflammasome with ASC. *Nature* **458,** 514–518 (2009).
23. Ishikawa, H. & Barber, G. N. STING is an endoplasmic reticulum adaptor that facilitates innate immune signalling. *Nature* **455,** 674–678 (2008).
24. Ishikawa, H., Ma, Z. & Barber, G. N. STING regulates intracellular DNA-mediated, type I interferon-dependent innate immunity. *Nature* **461,** 788–792 (2009).
25. Ishii, K. J. *et al.* A Toll-like receptor-independent antiviral response induced by double-stranded B-form DNA. *Nat. Immunol.* **7,** 40–48 (2006).
26. Kato, H. *et al.* Length-dependent recognition of double-stranded ribonucleic acids by retinoic acid-inducible gene-I and melanoma differentiation-associated gene 5. *J. Exp. Med.* **205,** 1601–1610 (2008).
27. Kawai, T. *et al.* IPS-1, an adaptor triggering RIG-I- and Mda5-mediated type I interferon induction. *Nat. Immunol.* **6,** 981–988 (2005).
28. Yanai, H. *et al.* HMGB proteins function as universal sentinels for nucleic-acid-mediated innate immune responses. *Nature* **462,** 99–103 (2009).
29. Smith-Garvin, J. E., Koretzky, G. A. & Jordan, M. S. T cell activation. *Annu. Rev. Immunol.* **27,** 591–619 (2009).
30. Marichal, T. *et al.* DNA released from dying host cells mediates aluminum adjuvant activity. *Nat. Med.* **17,** 996–1002 (2011).
31. Negishi, H. *et al.* Cross-interference of RLR and TLR signaling pathways modulates antibacterial T cell responses. *Nat. Immunol.* **13,** 659–666 (2012).
32. Zheng, W. & Flavell, R. A. The transcription factor GATA-3 is necessary and sufficient for Th2 cytokine gene expression in CD4 T cells. *Cell* **89,** 587–596 (1997).
33. Hwang, E. S., Szabo, S. J., Schwartzberg, P. L. & Glimcher, L. H. T helper cell fate specified by kinase-mediated interaction of T-bet with GATA-3. *Science* **307,** 430–433 (2005).
34. Afkarian, M. *et al.* T-bet is a STAT1-induced regulator of IL-12R expression in naive CD4+ T cells. *Nat. Immunol.* **3,** 549–557 (2002).
35. Noben-Trauth, N., Hu-Li, J. & Paul, W. E. Conventional, naive CD4+ T cells provide an initial source of IL-4 during Th2 differentiation. *J. Immunol.* **165,** 3620–3625 (2000).
36. Desmet, C. J. & Ishii, K. J. Nucleic acid sensing at the interface between innate and adaptive immunity in vaccination. *Nat. Rev. Immunol.* **12,** 479–491 (2012).
37. Pichlmair, A. *et al.* Activation of MDA5 requires higher-order RNA structures generated during virus infection. *J. Virol.* **83,** 10761–10769 (2009).
38. Monroe, K. M. *et al.* IFI16 DNA sensor is required for death of lymphoid CD4 T cells abortively infected with HIV. *Science* **343,** 428–432 (2014).
39. Doitsh, G. *et al.* Cell death by pyroptosis drives CD4 T-cell depletion in HIV-1 infection. *Nature* **505,** 509–514 (2014).
40. Berg, R. K. *et al.* T cells detect intracellular DNA but fail to induce Type I IFN responses: implications for restriction of HIV replication. *PloS One* **9,** e84513 (2014).
41. Goriely, S., Neurath, M. F. & Goldman, M. How microorganisms tip the balance between interleukin-12 family members. *Nat. Rev. Immunol.* **8,** 81–86 (2008).
42. Kim, S. *et al.* Cutting edge: basophils are transiently recruited into the draining lymph nodes during helminth infection via IL-3, but infection-induced Th2 immunity can develop without basophil lymph node recruitment or IL-3. *J. Immunol.* **184,** 1143–1147 (2010).
43. Yagi, R. *et al.* The IL-4 production capability of different strains of naive CD4(+) T cells controls the direction of the T(h) cell response. *Int. Immunol.* **14,** 1–11 (2002).
44. Liu, Z. *et al.* IL-2 and autocrine IL-4 drive the *in vivo* development of antigen-specific Th2 T cells elicited by nematode parasites. *J. Immunol.* **174,** 2242–2249 (2005).
45. Jankovic, D. *et al.* In the absence of IL-12, CD4(+) T cell responses to intracellular pathogens fail to default to a Th2 pattern and are host protective in an IL-10(-/-) setting. *Immunity* **16,** 429–439 (2002).
46. Kool, M. *et al.* An unexpected role for uric acid as an inducer of T helper 2 cell immunity to inhaled antigens and inflammatory mediator of allergic asthma. *Immunity* **34,** 527–540 (2011).
47. Schorn, C. *et al.* Monosodium urate crystals induce extracellular DNA traps in neutrophils, eosinophils, and basophils but not in mononuclear cells. *Front. Immunol.* **3,** 277 (2012).
48. Juncadella, I. J. *et al.* Apoptotic cell clearance by bronchial epithelial cells critically influences airway inflammation. *Nature* **493,** 547–551 (2013).
49. Ohtsuka, M. *et al.* NFAM1, an immunoreceptor tyrosine-based activation motif-bearing molecule that regulates B cell development and signaling. *Proc. Natl Acad. Sci. USA* **101,** 8126–8131 (2004).
50. Tanaka, S. *et al.* The enhancer HS2 critically regulates GATA-3-mediated Il4 transcription in T(H)2 cells. *Nat. Immunol.* **12,** 77–85 (2011).

Acknowledgements

We thank S. Yamasaki, T. Yokosuka, S. Tsukumo, A. Takeuchi, R. Onishi, H. Ike, Y. Motomura and M. Kubo for discussions and experimental help, M. Sakuma, M. Unno and A. Fujii for technical support, and H. Yamaguchi, M. Yoshioka and S. Kato for secretarial assistance. This work was supported by a Grant-in-Aid for Scientific Research from the Ministry of Education, Culture, Sports, Science and Technology of Japan (JSPS KAKENHI Grant numbers 24790489 for T.I. and 24229004 for T.S.).

Authors contributions

T.I. designed and performed the experiments and wrote the paper; C.I., M.E.S.G.B., Y.K., A.H-T. and H.H performed the experiments; T.K., O.T., K.J.I., S.T., T.N., F.B., G.N.B. and S.A. provided knockout mice; T.S. designed the experiments and wrote the paper.

Additional information

Supplementary Information accompanies this paper at http://www.nature.com/naturecommunications

Competing financial interests: The authors declare no competing financial interests.

Reprints and permission information is available online at http://npg.nature.com/reprintsandpermissions/

How to cite this article: Imanishi, T. *et al.* Nucleic acid sensing by T cells initiates Th2 cell differentiation. *Nat. Commun.* 5:3566 doi: 10.1038/ncomms4566 (2014).

Published OnlineFirst March 3, 2014; DOI: 10.1158/0008-5472.CAN-13-1703

Microenvironment and Immunology

Cancer Research

RAE1 Ligands for the NKG2D Receptor Are Regulated by STING-Dependent DNA Sensor Pathways in Lymphoma

Adeline R. Lam[1,2], Nina Le Bert[1], Samantha S.W. Ho[1], Yu J. Shen[1,2], Melissa L.F. Tang[1], Gordon M. Xiong[1], J. Ludovic Croxford[1], Christine X. Koo[1,2,3,4], Ken J. Ishii[3,4], Shizuo Akira[5], David H. Raulet[6], and Stephan Gasser[1,2]

Abstract

The immunoreceptor NKG2D originally identified in natural killer (NK) cells recognizes ligands that are upregulated on tumor cells. Expression of NKG2D ligands (NKG2DL) is induced by the DNA damage response (DDR), which is often activated constitutively in cancer cells, revealing them to NK cells as a mechanism of immunosurveillance. Here, we report that the induction of retinoic acid early transcript 1 (RAE1) ligands for NKG2D by the DDR relies on a STING-dependent DNA sensor pathway involving the effector molecules TBK1 and IRF3. Cytosolic DNA was detected in lymphoma cell lines that express RAE1 and its occurrence required activation of the DDR. Transfection of DNA into ligand-negative cells was sufficient to induce RAE1 expression. *Irf3*$^{+/-}$;Eμ-*Myc* mice expressed lower levels of RAE1 on tumor cells and showed a reduced survival rate compared with *Irf3*$^{+/+}$;Eμ-*Myc* mice. Taken together, our results suggest that genomic damage in tumor cells leads to activation of STING-dependent DNA sensor pathways, thereby activating RAE1 and enabling tumor immunosurveillance. *Cancer Res; 74(8); 2193–203. ©2014 AACR.*

Introduction

The NKG2D system is an arm of innate immune recognition, which is important in the context of both cancer and infection (1–3). Transformed and infected cells increase their expression of NKG2D ligands (NKG2DL). Engagement of the NKG2D receptor on natural killer (NK) cells and certain T cells stimulates their effector functions, which aid in tumor control (4, 5). Recently, we elucidated a principle mechanism that induces NKG2DLs in cancer cells: the DNA damage response (DDR; ref. 6). DNA damage upregulates the expression of numerous NKG2DLs, including different retinoic acid early transcript (RAE1) isoforms and mouse UL16-binding protein-like transcript 1 (MULT1) in mouse cells. The DDR molecules ataxia telangiectasia and Rad3 related (ATR) ataxia telangiectasia mutated homolog (ATM), and checkpoint kinase 1 homolog (CHK1) are required for expression of NKG2DLs in response to DNA damage and the constitutive expression of NKG2DLs in some tumor cell lines (6). Additional effector molecules of the DDR required for mouse NKG2DL expression have not been identified.

Optimal immune responses to autologous cells often require the presence of pathogen- and damage-associated molecular patterns. Pattern recognition receptors (PRR) that recognize self-molecules, such as DNA, have been suggested to play a role in cancer (7). Recently identified candidate cytosolic DNA sensors include Z-DNA binding protein 1 (ZBP1/DAI) and retinoic acid inducible gene I (Rig-I; ref. 8). Upon recognizing DNA, these sensors activate stimulator of interferon (IFN) genes (STING), TANK-binding kinase 1 (TBK1), and/or the related IKK-related kinase epsilon (IKKε; ref. 9). Activated TBK1 and IKKε directly phosphorylate IFN regulatory factor-3 (IRF3), which subsequently undergoes dimerization and translocation into the nucleus (10). Nuclear IRF3 induces the expression of target genes, including *Ifnb* and chemokine C-C motif ligand-5 (*Ccl5*; ref. 11).

Expression of the proto-oncogene c-*MYC* is deregulated in 70% of human cancers (12, 13). Overexpression of c-*MYC* induces DNA damage and the DDR, which was suggested to act as a barrier against tumor development in premalignant cells. In Eμ-*Myc* transgenic mice, c-*Myc* expression is driven by the immunoglobulin heavy chain Eμ enhancer, leading to precursor B-cell malignancies similar to human Burkitt's lymphoma (14, 15). The tumor suppressors that prevent the development of c-*Myc*–expressing premalignant cells have not been well characterized.

In the present study, we show that the DDR leads to the presence of cytosolic DNA and activation of IRF3 in lymphoma cell lines. The induction of RAE1 ligands by the DDR depended on IRF3. Transfection of cells with cytosolic DNA induced the

Authors' Affiliations: [1]Immunology Programme and Department of Microbiology, Centre for Life Sciences; [2]NUS Graduate School for Integrative Sciences and Engineering, National University of Singapore, Singapore; [3]Laboratory of Adjuvant Innovation, National Institute of Biomedical Innovation (NIBIO); [4]Laboratory of Vaccine Science, [5]WPI Immunology Frontier Research Center (iFREC), Osaka University, Suita, Osaka, Japan; and [6]Department of Molecular and Cell Biology and Cancer Research Laboratory, University of California, Berkeley, California

Note: Supplementary data for this article are available at Cancer Research Online (http://cancerres.aacrjournals.org/).

D.H. Raulet and S. Gasser contributed equally to this article.

Corresponding Author: S. Gasser, Immunology Programme, Centre for Life Sciences, #03-05, 28 Medical Drive, 117456 Singapore. Phone: 6565167209; Fax: 6567782684; E-mail: micsg@nus.edu.sg

doi: 10.1158/0008-5472.CAN-13-1703

Published OnlineFirst March 3, 2014; DOI: 10.1158/0008-5472.CAN-13-1703

expression of RAE1 molecules. Tumors in *Irf3*$^{+/-}$;Eμ-*Myc* mice expressed lower levels of RAE1 and developed lymphoma earlier, resulting in a shortened life span when compared with *Irf3*$^{+/+}$;Eμ-*Myc* mice. Taken together, these findings link genotoxic stress to cytosolic DNA sensor signaling pathways and the induction of RAE1 in lymphoma cell lines.

Materials and Methods

Cells

BC2 (a kind gift by Dr. L. Corcoran, Walter+Eliza Hall Institute of Medical Research, Parkville, Victoria, Australia) and EμM1 cells were derived from Eμ-*Myc* mice (16). Yac-1 cells were purchased from American Type Culture Collection. Cells were cultured in RPMI-1640 medium (Invitrogen) with 10% FCS (Hyclone), 50 μmol/L 2-mercaptoethanol, 100 μmol/L asparagine, 2 mmol/L glutamine (Sigma), 1% penicillin-streptomycin (Invitrogen), and 1/1,000 plasmocin (Invivogen).

EμM1, mouse embryonic fibroblasts (MEF), and tumor cells in Eμ-*Myc* mice (C57BL/6) express RAE1βδ and/or RAE1ε. BC2 (C57BL/6/129) and Yac-1 (A/Sn) cells express RAE1α, RAE1β, RAE1γ, and RAE1δ.

Reagents

Aphidicolin, caffeine, CGK733, cytosine β-D-arabinofuranoside hydrochloride (Ara-C), Dimethyl sulfoxide (DMSO), Poly G:C, Poly A:U, and Poly I:C were purchased from Sigma. TransFectin was purhased from BioRad. KU55933 and VE-821 were obtained from Tocris Bioscience or Axon Medchem. ODN1585, ODN1668 control (ssDNA), and lipopolysaccharides (LPS) were purchased from Invivogen. DNA was conjugated to Alexa-488 using the Ulysis labeling kit according to the manufacturer's instructions (Invitrogen).

Constructs and transduction

Irf3, *Tbk1*, *Ikke*, *Sting*-HA, *IRF3-Egfp*, and *IRF3A7-Egfp* were subcloned into the pMSCV2.2-IRES-*Gfp* vector (gift of Dr. Sha, University of California, Berkeley, CA). Wild-type (WT) and mutant *Sting* fibroblasts were kindly provided by Dr. Vance (University of California, Berkeley, CA). Retroviral supernatants were generated as described in (17). Short hairpin RNA (shRNA) constructs were cloned into the MSCV/LTRmiR30-PIG vector (Open Biosystems; See Supplementary data).

Quantitative real-time reverse transcription PCR

Quantitative real-time reverse transcription (RT)-PCR was performed as described previously (6).

Western blotting

Whole cell extracts were electrophoresed in 10% or 4% to 20% SDS-PAGE gels and blotted onto nitrocellulose membranes (BioRad). Antibodies against IRF3, IRF3pS396, TBK1, TBK1pS172, ATM, ATMpS1981 (Cell Signaling Technology), BCL2L12 (clone E-13; Santa Cruz), and glyceraldehyde-3-phosphate dehydrogenase (GAPDH; Sigma) and horseradish peroxidase–coupled second stage reagents were used (Thermo). Blots were exposed on X-ray film (Fuji); densitometry analysis was performed using ImageJ-1.46r.

Flow cytometry

The following antibodies were used: pan-RAE1, RAE1αβγ, RAE1βδ, RAE1ε (R&D Systems), B220-PerCP, IgM-APC, CD16/CD32, MHC class II (eBioscience), rabbit-anti-phospho-IRF3-Ser396 or rabbit-anti-phospho-TBK1-Ser172 (Cell Signaling Technology), and rat IgG-APC (eBioscience) or rabbit IgG-Alexa-488 (Invitrogen). Propidium iodide (PI, 1 μg/mL) was added to all stainings, and PI-negative cells are shown. For intracellular staining, cells were fixed according to the manufacturer's protocol. Some cells were treated with 2 U/μL λ-phosphatase (New England Biolabs) at 37°C for 90 minutes before staining. Stained cells were analyzed using FACSCalibur and FlowJo 8.8.7 (Treestar). Bromodeoxyuridine incorporation analysis was performed as described (18).

Microscopy

Cells were fixed and stained for DNA according to the manufacturer's instructions (Millipore). A detailed protocol is provided in the Supplementary data.

CD107a degranulation assay and *in vitro* NK cell stimulation

Performed as described in refs. 4 and 19.

Statistical analyses

Groups were compared using two-tailed unpaired *t* tests (Prism; 5.0c; GraphPad). Survival was represented by Kaplan–Meier curves, and statistical analysis was performed with the log-rank Mantel–Cox test.

Results

IRF3 is necessary for RAE1 expression in response to DNA damage

IRF3 has previously been shown to be activated in response to DNA damage (20, 21). We therefore investigated the role of IRF3 in the expression of NKG2DLs in cells exposed to DNA damaging agents. Phosphorylation of serine 396 (S388 of mouse IRF3) has been shown to be critical for the activation of IRF3 (22). Phosphorylation of IRF3S388 increased after treatment with DDR-inducing agents Ara-C or aphidicolin, although not to the same degree as LPS, a known inducer of IRF3 (Fig. 1A and B; Supplementary Fig. S1A; ref. 23). The late kinetics of IRF3S388 phosphorylation were similar to kinetics previously observed for DNA damage–induced upregulation of NKG2DLs (6). Notably, treatment of BC2 cells with Ara-C also induced activated IRF3 characterized by nuclear translocation of endogenous IRF3 (Fig. 1C) and overexpressed chimeric IRF3-GFP (Fig. 1D and E), consistent with previous reports (20, 21). No nuclear translocation was observed with a mutant form of IRF3 (IRF3A7-GFP) that is unable to be activated (Fig. 1D and E). Treatment of BC2 cells with Ara-C or aphidicolin induced expression of several IRF3 target genes to a similar or greater extent than Poly I:C, an established IRF3 activator, suggesting that IRF3 is transcriptionally active in response to DNA damage (Fig. 1F and G).

To test whether IRF3 is required for DDR-mediated upregulation of NKG2DLs, we transduced BC2 cells with an *Irf3*-specific shRNA (Supplementary Fig. S1B). Compared with

Published OnlineFirst March 3, 2014; DOI: 10.1158/0008-5472.CAN-13-1703

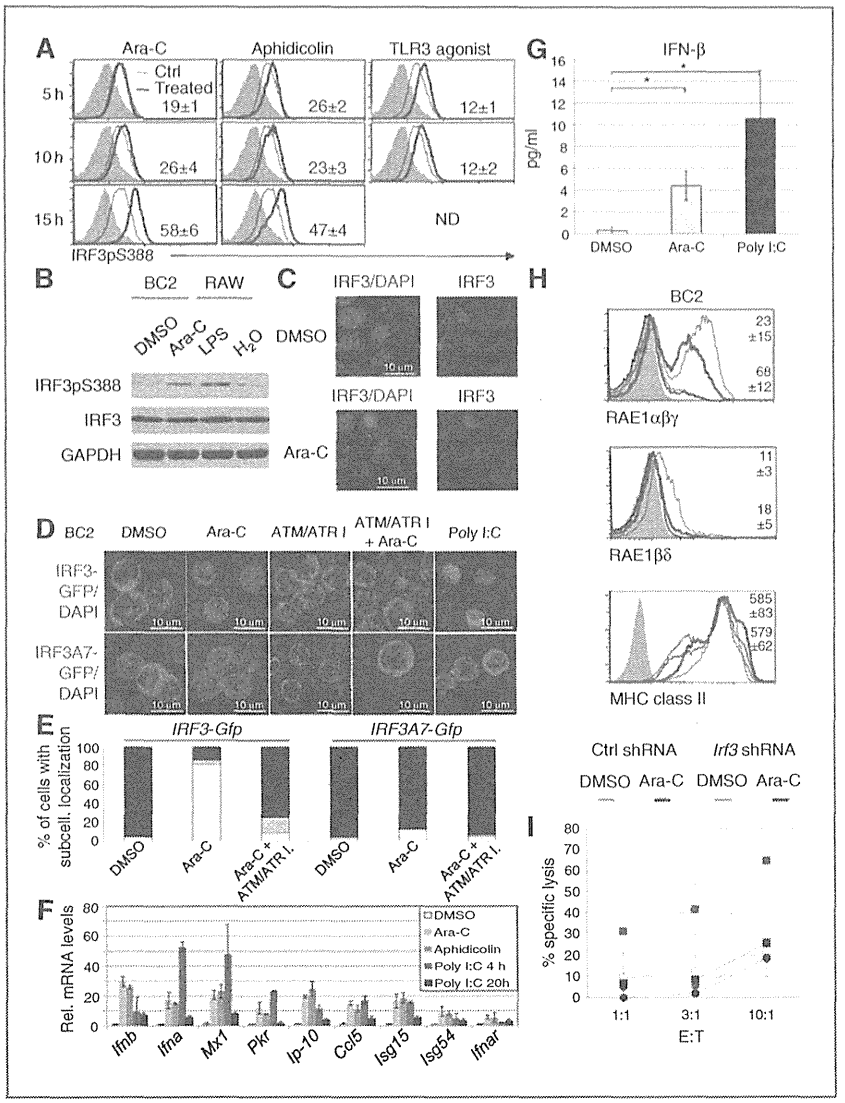

Figure 1. IRF3 is activated and necessary for optimal induction of RAE1 ligands for NKG2D in response to DNA damage. A, phosphorylation of IRF3S388 in BC2 cells treated with 10 μmol/L Ara-C, 4 μmol/L aphidicolin, 1 μg/mL ODN1585 (red line), or DMSO (blue line) was analyzed by intracellular flow cytometry at indicated time points. Filled histograms, isotype staining of Ara-C–treated cells. Mean fluorescence intensity (MFI) ±SD are shown. B, phosphorylation of IRF3S388 after 16 hours of 10 μmol/L Ara-C or DMSO treatment was analyzed by Western blotting. RAW 264.7 cells were treated with LPS for 4 hours. C, nuclear translocalization of endogenous IRF3 (red) in BC2 cells treated with 10 μmol/L Ara-C for 16 hours and stained for IRF3 in the presence of DAPI (blue). D and E, BC2 cells expressing *IRF3-Gfp* or *IRF3A7-Gfp* were treated with 10 μmol/L Ara-C, 10 μg/mL Poly I:C, or DMSO for 16 hours. Some cells were pretreated with 10 μmol/L of the ATM/ATR-specific inhibitor CGK733. Localization of IRF3 in DAPI-stained cells was analyzed by fluorescent microscopy (D). Quantification of BC2 cells with nuclear (white bar; >90% nuclear), partial nuclear (gray bar; 10%–90% nuclear) and cytosolic (black bar; <10% nuclear) localization of IRF3 (E). F, BC2 cells were treated with DMSO (white bar), 10 μmol/L Ara-C (light-gray bar), 4 μmol/L aphidicolin (gray bar), 1 μg/mL Poly I:C for 20 hours (black bar), or 1 μg/mL Poly I:C for 4 hours (dark-gray bar). Relative mRNA levels of IRF3 target genes were measured by qRT-PCR. Means ±SD of three independent experiments normalized to DMSO-treated cells are shown. G, levels of IFN-β in supernatants of 0.75×10^6 BC2 cells/mL treated with DMSO, 10 μmol/L Ara-C, or 1 μg/mL Poly I:C for 24 hours were determined by ELISA. *, $P < 0.05$. H, RAE1 expression in *Irf3*-specific (red line) or control (blue line) shRNA-transduced BC2 cells, which were cultured for 5 days in puromycin before treatment with 10 μmol/L Ara-C for 16 hours. DMSO-treated *Irf3* (dashed line) or control (dotted line) shRNA-transduced cells are also shown. Filled histograms, isotype staining of Ara-C–treated cells. MFI ±SD are indicated. I, IL-2–activated NK cells were cocultured with *Irf3*-specific (circles) or control shRNA-transduced (squares) BC2 cells in the presence of NKG2D-blocking antibodies (open symbols) or IgG2a isotype control antibodies (filled symbols) and treated with 10 μmol/L Ara-C (red) or DMSO (black) for 16 hours. The effector (E) to target (T) ratio is indicated. Results ±SD of three independent experiments are shown.

Published OnlineFirst March 3, 2014; DOI: 10.1158/0008-5472.CAN-13-1703

control shRNA, *Irf3*-specific shRNA significantly inhibited the upregulation of RAE1 ligands of NKG2D, but not MHC class II, in response to Ara-C (Fig. 1H). Bimodal expression of RAE1 is likely to reflect specific activation of the DDR in S-phase of the cell cycle. No consistent effects were observed for the NKG2DLs MULT-1 and H60, suggesting that their upregulation in response to DNA damage requires additional signals.

To address whether IRF3-induced RAE1 expression renders cells more sensitive to NK cell–mediated lysis, *Irf3*-specific and control shRNA-transduced cells were cultured with interleukin (IL)-2–activated NK cells. BC2 cells transduced with *Irf3*-specific shRNA were less sensitive to NK cell–mediated cytotoxicity in response to Ara-C treatment than control shRNA-transduced BC2 cells (Fig. 1I). The sensitivity of *Irf3*-shRNA–transduced BC2 cells was similar to control shRNA-transduced BC2 cells treated with Ara-C in the presence of NKG2D-blocking antibodies, suggesting that decreased lysis of *Irf3*-shRNA–transduced cells was due to reduced RAE1 expression.

IRF3 is required for constitutive RAE1 expression in Yac-1 cells

The DDR is constitutively activated in many tumor cell lines and precancerous lesions (24). In agreement, phosphorylation of IRF3S388 was detected in EμM1 cells and Yac-1 lymphoma cells (Fig. 2A). Endogenous IRF3 (Fig. 2B) and exogenous chimeric IRF3-GFP (Fig. 2C) were partially localized to the nucleus, indicating that a subset of IRF3 is activated in EμM1 and Yac-1 cells. In contrast, IRF3A7 exhibited exclusively cytosolic localization in Yac-1 cells. Inhibition of IRF3 expression in EμM1 and Yac-1 cells by shRNA decreased the expression of IRF3 target genes (Fig. 2D and E), *Raet1* transcripts (Supplementary Fig. S1C), and RAE1 cell surface levels (Fig. 2F). Mouse strains were found to express different RAE1 isoforms and the cell lines used in this study vary in their genetic background (see Supplementary Materials and Methods; ref. 25). The incomplete reduction of cell surface RAE1 expression by *Irf3*-specific shRNAs may reflect incomplete turnover of preformed RAE1 or incomplete knockdown of IRF3 (Supplementary Fig. S1B).

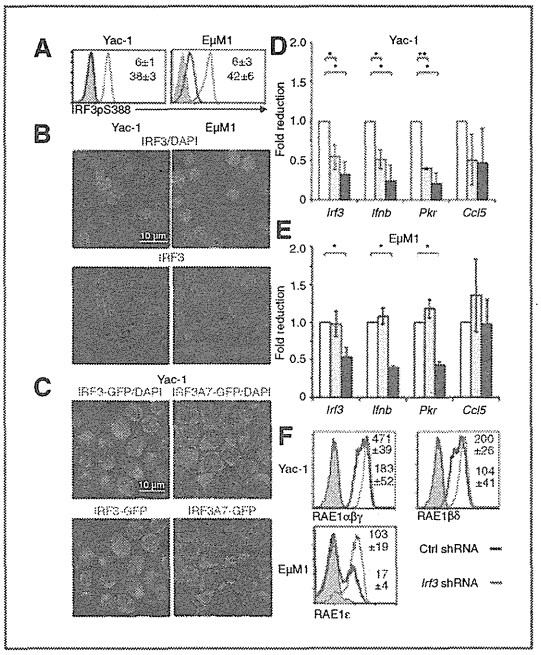

Figure 2. IRF3 is necessary for constitutive RAE1 expression in Yac-1 and EμM1 cells. A, expression of IRF3pS388 in Yac-1 and EμM1 cells was detected by intracellular flow cytometry (blue line). Some cells were pretreated with λ-phosphatase before staining (red line). Filled histogram, isotype staining of Yac-1 cells. MFI ±SD are indicated. B, Yac-1 and EμM1 cells were stained for endogenous IRF3 (red) and DAPI (blue). C, *IRF3-Gfp* or *IRF3A7-Gfp*–transduced Yac-1 cells were examined by confocal microscopy for GFP expression in the presence of DAPI (blue). D and E, relative transcript levels of IRF3 target genes in *Irf3*-specific (gray and black bars) or control shRNAs (white bar)-transduced Yac-1 (D) and EμM1 (E) cells were analyzed by qRT-PCR. Means ±SD of three independent experiments normalized to control shRNA-transduced cells are shown. *, $P < 0.05$; **, $P < 0.01$. F, RAE1 expression in *Irf3*-specific (red line) or control (blue line) shRNA-transduced Yac-1 or EμM1 cells 5 days after selection in puromycin. Isotype control staining of *Irf3*- (dotted line) or control shRNA- (filled histogram) transduced cells is shown. MFI ±SD are indicated.

TBK1 is necessary for RAE1 expression in response to DNA damage

IRF3 is activated by the IKK-related serine/threonine kinases TBK1 and IKKε (10). We therefore tested whether TBK1 was phosphorylated in response to DNA damage. Similar to results with IRF3, substantial phosphorylation of TBK1 on serine 172 was detected after 15 hours of treatment with Ara-C or aphidicolin, although the activation was weaker than TBK1 phosphorylation in response to LPS (Fig. 3A and B; Supplementary Fig. S2A). No *Ikke* expression was detected in BC2 cells (data not shown).

Transduction of BC2 cells with the TBK1 inhibitor *Sike* caused substantial reduction in RAE1 expression in response to DNA damage (Fig. 3C). Similarly, BC2 cells transduced with *Tbk1*-specific shRNA expressed less transcripts and RAE1 at the cell surface in response to Ara-C (Fig. 3D; Supplementary Fig. S2B). *Tbk1*- and *Ikke*-deficient MEFs failed to upregulate RAE1 in response to Ara-C (Fig. 3E). Genetic reconstitution of *Tbk1*$^{-/-}$:*Ikke*$^{-/-}$ MEFs with *Tbk1* or *Ikke* was sufficient to induce RAE1 expression on a fraction of cells and to restore the capacity of cells to upregulate RAE1 in response to Ara-C (Fig. 3E). The induction of RAE1 in untreated cells is likely a consequence of overexpression of *Tbk1* or *Ikke*, which has been shown to result in unregulated activation of the pathway (26). In summary, the data suggest that TBK1 is required for induction of RAE1 in response to DNA damage in BC2 cells.

TBK1 is required for constitutive RAE1 expression

Similarly to IRF3, constitutive phosphorylation of TBK1S172 was detected in Yac-1 and EμM1 cells (Fig. 3F). Transduction of *Sike* into Yac-1 cells caused reductions in RAE1 levels (Fig. 3G). Expression of a *Tbk1*-specific shRNA in Yac-1 cells decreased the amount of *Raet1* transcripts, and a significant but less complete reduction in RAE1 at the cell

Published OnlineFirst March 3, 2014; DOI: 10.1158/0008-5472.CAN-13-1703

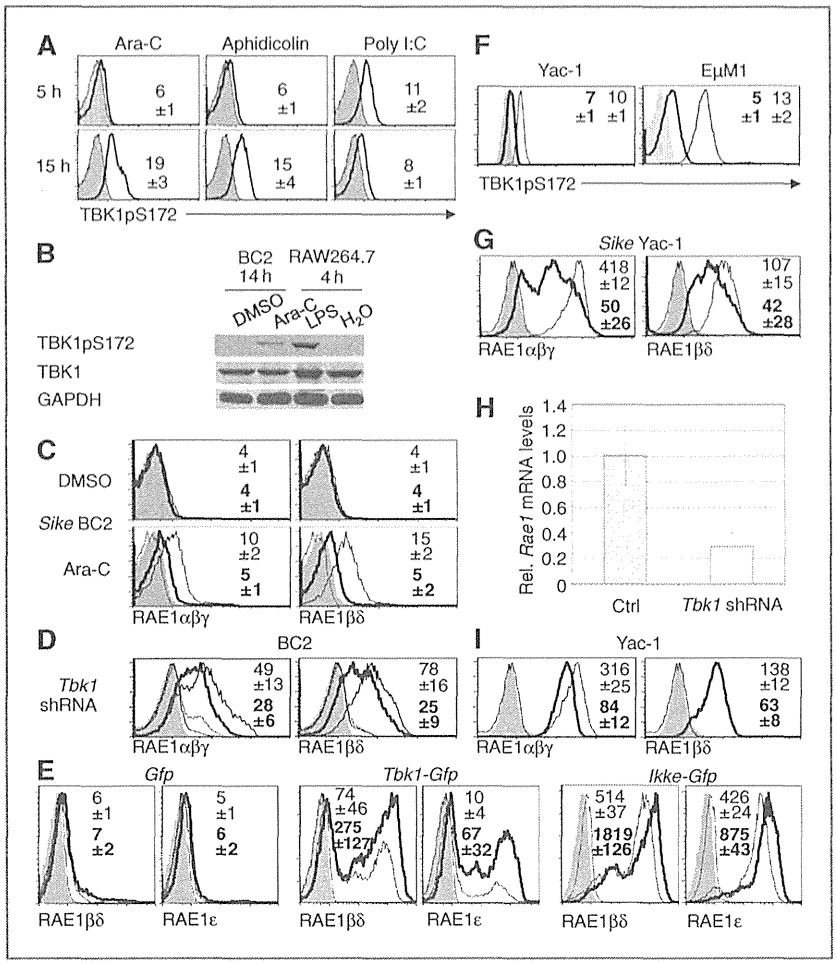

Figure 3. Expression of RAE1 depends on TBK1. A, levels of TBK1S172 phosphorylation in BC2 cells treated as indicated in Fig. 1A (bold line) or DMSO (fine line). Filled histograms, isotype staining of DMSO-treated cells. B, immunoblot analysis of TBK1S172 phosphorylation in 10 μmol/L Ara-C (14 hours) or DMSO-treated BC2 cells. RAW 264.7 cells were treated with LPS for 4 hours for comparison. C, BC2 cells were transduced with retroviral vectors encoding *Sike* (bold line) or control vector (fine line). Ten days posttransduction, BC2 cells were treated with 10 μmol/L Ara-C or DMSO for 16 hours and stained for RAE1. Isotype staining of control- (dashed line) or *Sike*- (filled histogram) transduced cells is shown. D, RAE1 expression in *Tbk1*-specific (bold lines) or control (fine line) shRNA-transduced BC2 cells treated with 10 μmol/L Ara-C for 16 hours. *Tbk1*-specific (dashed line) or control (dotted line) shRNA-transduced cells treated with DMSO were also stained for RAE1 expression. Filled histogram, isotype control of Ara-C–treated cells. E, *Tbk1*$^{-/-}$;*Ikke*$^{-/-}$ MEFs were transduced with retroviral vectors encoding *Tbk1*, *Ikke*, or with empty vector. Eight days after selection, cells were treated with 10 μmol/L Ara-C for 16 hours (bold line) or DMSO (fine line) and analyzed for the expression of indicated NKG2DLs. Isotype stainings of DMSO (filled histogram) or Ara-C–treated (dashed line) are shown. F, levels of TBK1S172 phosphorylation in Yac-1 cells were analyzed by intracellular flow cytometry (fine line). Some cells were pretreated with λ-phosphatase before staining (bold line). Filled histogram, isotype staining of Yac-1 cells. G, RAE1 expression in *Sike*-encoding vector (bold line) or empty vector–transduced Yac-1 cells (fine line) 10 days posttransduction. Filled histogram, isotype stainings of *Sike*-expressing cells. Dashed line, isotype control of empty vector–transduced cells. H, levels of *Rae1* transcripts were determined by qRT-PCR in *Tbk1*-specific (open bar) or control (filled bar) shRNA-transduced Yac-1 cells 5 days posttransduction. Means ±SD for three independent experiments are shown. I, RAE1 expression in *Tbk1*-specific (bold line) or control (fine line) shRNA-transduced Yac-1 cells. Isotype staining of *Tbk1*-specific (dashed line) and control (filled histogram) shRNA-transduced cells is shown. MFI ± SD are indicated.

surface (Fig. 3H and I). No *Ikke* transcripts were detected in Yac-1 cells (data not shown).

Phosphorylation of IRF3 and TBK1 depends on the DDR

Treatment of cells with Ara-C results in DNA breaks and the activation of ATR and ATM (27). To address the role of ATM and ATR in the activation of TBK1 and IRF3, we blocked ATM and ATR function with different chemical inhibitors. Attempts to efficiently block both ATM and ATR by shRNA were not successful. Induction of RAE1 expression in BC2 cells by Ara-C was inhibited by the combined treatment of cells with ATM and ATR inhibitors (Fig. 4A; Supplementary Fig. S3A).

Published OnlineFirst March 3, 2014; DOI: 10.1158/0008-5472.CAN-13-1703

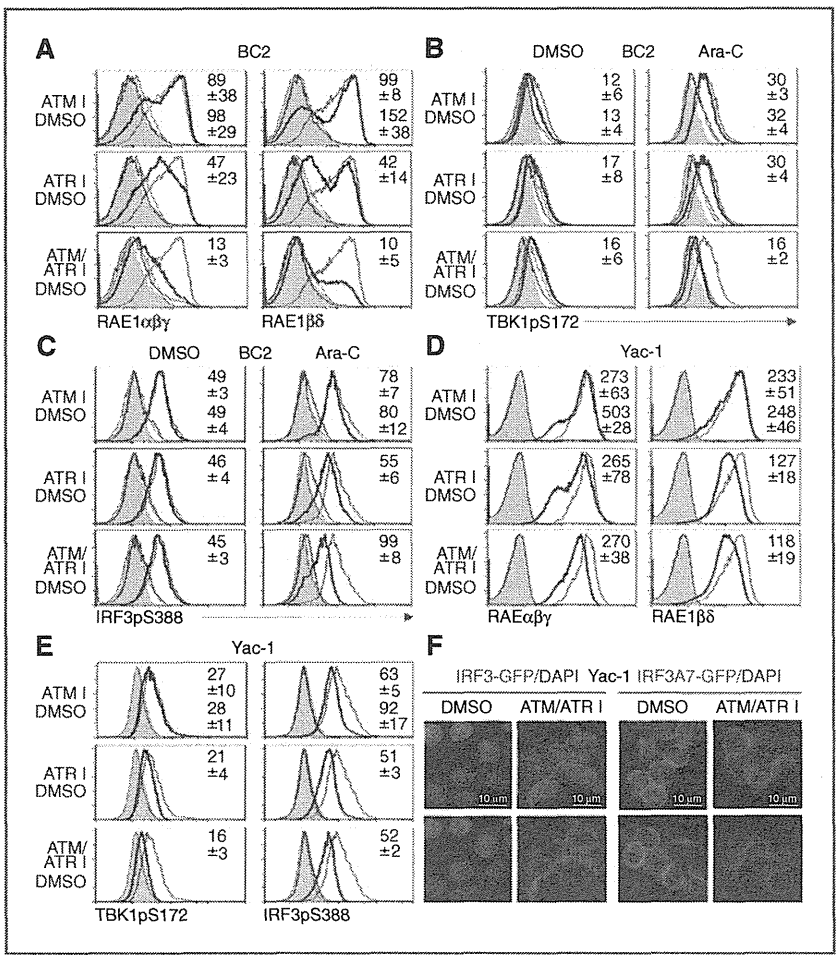

Figure 4. ATR-dependent activation of TBK1 and IRF3 in response to DNA damage. A–C, analysis of RAE1 expression (A), phosphorylation of TBK1S172 (B), and IRF3S388 (C) in 10 μmol/L Ara-C–treated (16 hours) BC2 cells pretreated with 10 μmol/L of the ATM inhibitor KU55933, the ATR inhibitor VE-821, KU55933+VE-821 (red line), or DMSO (blue line). Control cells were pretreated with the same inhibitors (dashed line) or DMSO (fine line) before DMSO treatment. Filled histograms, isotype control staining. MFI ±SD are indicated. D and E, Yac-1 cells treated with ATM and/or ATR-specific inhibitors (red line) or DMSO (blue line) for 16 hours as indicated above were stained for RAE1 (D), TBK1pS172 (left), and IRF3pS388 (right; E). Filled histograms, isotype control stainings. MFI ±SD are indicated. F, *IRF3-Gfp* or *IRF3A7-Gfp*–transduced Yac-1 cells were treated with 10 μmol/L of KU55933+VE-821 or DMSO for 14 hours. IRF3 expression and DAPI (blue) staining was analyzed by fluorescent microscopy.

Inhibition of ATM and ATR also impaired TBK1 and IRF3 phosphorylation (Fig. 4B and C; Supplementary Fig. S3B) and nuclear localization of chimeric IRF3-GFP (Fig. 1D and E) in Ara-C–treated BC2 cells. The effects of ATM or ATR inhibition on RAE1 expression and phosphorylation of TBK1 and IRF3 were less pronounced, suggesting that ATM and ATR act redundantly (Fig. 4A–C).

Inhibition of ATR impaired constitutive RAE1 expression and phosphorylation of TBK1 and IRF3 in Yac-1 cells (Fig. 4D and E, Supplementary Figs. S3C and S3D). Nuclear localization of IRF3-GFP in Yac-1 cells was also suppressed by inhibition of ATR and ATM (Fig. 4F). Thus, activation of TBK1 and IRF3 in Yac-1 cells depends on ATR, suggesting that ATR activates DNA damage, which preferentially activates ATR, is present in Yac-1 cells (28).

Accumulation of cytosolic DNA depends on the DDR

Recognition of cytosolic DNA by DNA sensors activates TBK1 and IRF3 (8). To test whether DNA damage leads to appearance of cytosolic DNA, we stained cells with antibodies specific for single-stranded (ss) DNA or double-stranded (ds) DNA (Supplementary Fig. S4A). The specificity of the DNA staining was verified by pretreating cells with S1 nuclease to degrade ssDNA or DNase I to digest dsDNA before staining (Supplementary Figs. S4B and S4C). All cells were treated with RNase before staining. Strikingly, we found that ssDNA and dsDNA was present in the cytosol of BC2 cells in response to Ara-C treatment and cytosolic DNA was constitutively present in Yac-1 cells (Fig. 5A and B). To substantiate the presence of DNA in the cytosol of cells, we stained BC2 cells with PicoGreen, a vital dsDNA-specific dye (Supplementary Fig. S4D). In agreement with the dsDNA-specific antibody stainings, PicoGreen staining showed the presence of cytosolic dsDNA in Yac-1 and Ara-C–treated BC2 cells (Fig. 5C; Supplementary Figs. S5A and S5B). To exclude the possibility that cytosolic DNA represents mitochondrial DNA, we costained cells with mitochondria-specific MitoTracker dye or the mitochondrial marker COX-IV (Fig. 5C, Supplementary Figs. S4–S6). As Ara-C disrupted MitoTracker staining, we treated BC2 cells with aphidicolin, an

Published OnlineFirst March 3, 2014; DOI: 10.1158/0008-5472.CAN-13-1703

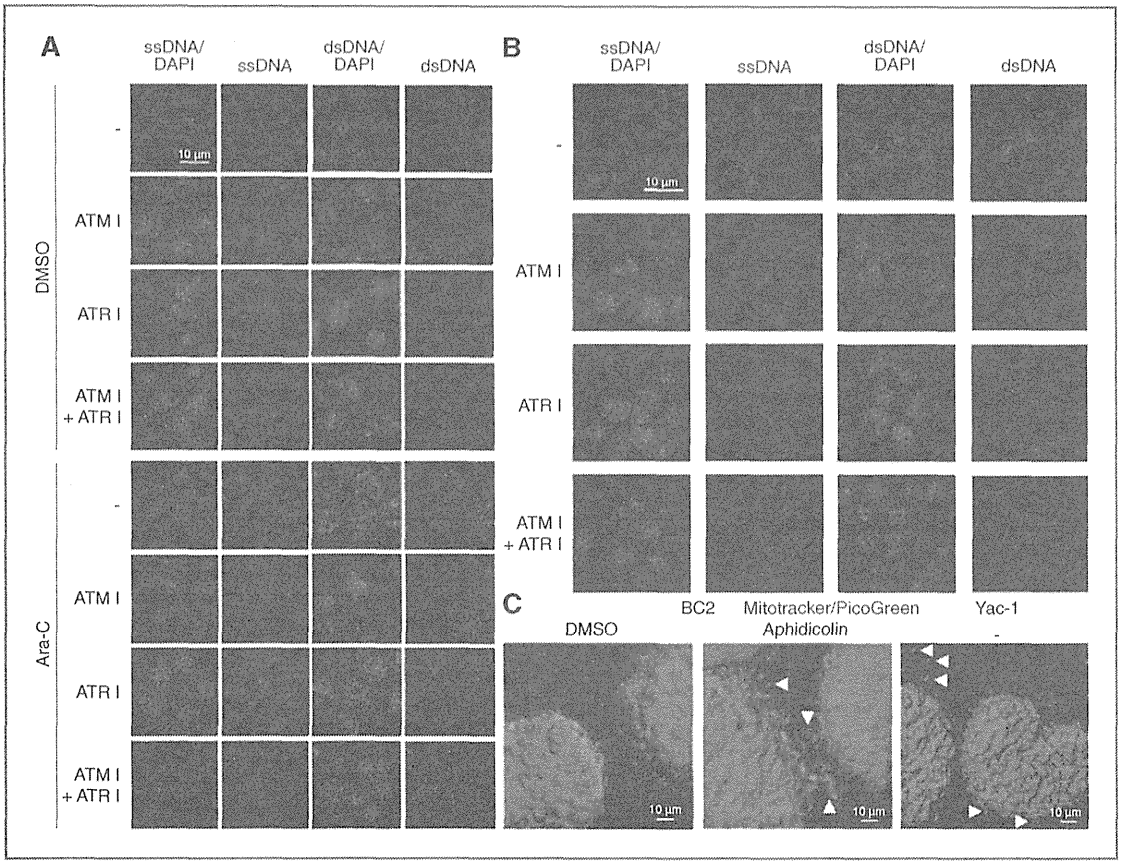

Figure 5. DNA damage leads to the appearance of cytosolic DNA. A, staining of BC2 cells for the presence of ssDNA (left columns) or dsDNA (right columns) in the presence of DAPI (first and third column). BC2 cells were pretreated with 10 μmol/L of the ATM inhibitor KU55933, the ATR inhibitor VE-821, KU55933+VE-821, or DMSO followed by treatment with DMSO or 10 μmol/L Ara-C for 14 hours. BC2 cells were treated with RNase and stained with ssDNA- or dsDNA-specific antibodies (red) and DAPI (blue). B, Yac-1 cells were treated with 10 μmol/L KU55933, VE-821, KU55933+VE-821, or DMSO for 14 hours and stained as outlined in A. C, DMSO (left) or 4 μmol/L aphidicolin-treated (middle; 14 hours) BC2 cells and Yac-1 cells (right) were incubated with the dsDNA-specific dye PicoGreen (green) for 1 hour and MitoTracker dye (red) for 15 minutes. Z-stack images were acquired by confocal microscopy and analyzed using Imaris software to generate iso-surface plots. White arrows, presence of cytosolic DNA.

inhibitor of nuclear DNA synthesis that activates the DDR but does not affect replication of mitochondrial DNA (Fig. 5C; Supplementary Fig. S4D; ref. 29). Three-dimensional rendering of confocal microscopy data showed that most cytosolic DNA is present outside of mitochondria in Yac-1 and Ara-C–treated BC2 cells (Fig. 5C; Supplementary Figs. S4D and S5).

To test whether the DDR influences the occurrence of cytosolic DNA, we pretreated BC2 cells with ATM and/or ATR inhibitors before treatment with Ara-C. Blocking of ATM and ATR prevented appearance of cytosolic DNA in response to Ara-C (Fig. 5A; Supplementary Fig. S6A). Strikingly, cytosolic DNA present in Yac-1 cells disappeared after inhibition of ATR for 14 hours (Fig. 5B; Supplementary Fig. S6B). Inhibition of ATM had a less pronounced effect on the occurrence of cytosolic DNA in agreement with effects observed on RAE1 expression and phosphorylation of IRF3 and TBK1 (Fig. 5A and B). However, the disappearance of cytosolic DNA in response to inhibition of ATM and ATR did not abrogate RAE1 expression in Yac-1 cells, suggesting that RAE1 expression is regulated by additional pathways (25). In summary, our data suggest that appearance of cytosolic DNA depends on the DDR and is rapidly turned over.

Cytosolic DNA induces RAE1 expression

To test whether cytosolic DNA induces RAE1 expression in BC2 cells, we transfected cells with Alexa-488–labeled plasmid DNA, genomic DNA, or ssDNA. We were unable to purify sufficient quantities of cytosolic DNA to determine whether cytosolic DNA present in Ara-C–treated BC2 cells directly induces RAE1 expression. Alexa-488–positive BC2 cells upregulated expression of RAE1, although to a lesser degree than Ara-C–treated cells (Fig. 6A).

The presence of DNA in the cytosol activates STING-dependent DNA sensors, leading to the activation of TBK1 and

Published OnlineFirst March 3, 2014; DOI: 10.1158/0008-5472.CAN-13-1703

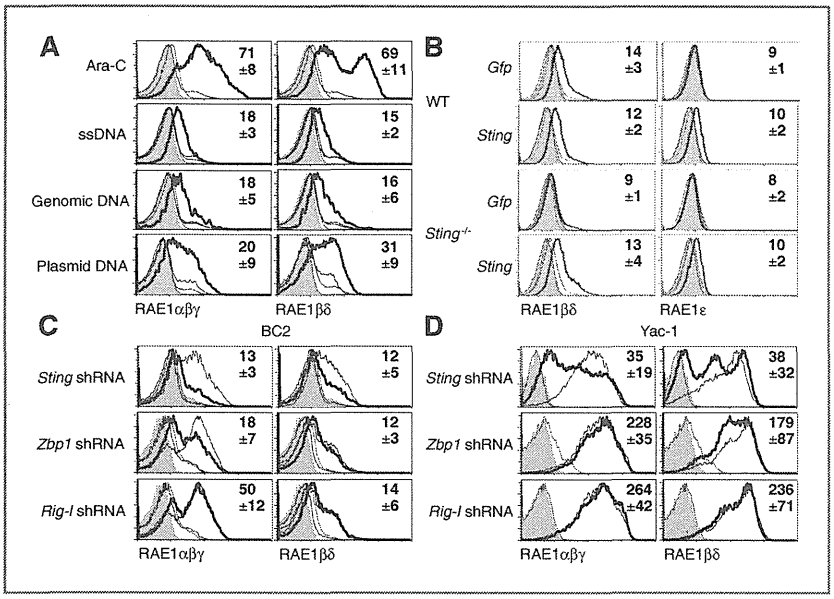

Figure 6. RAE1 expression is induced by cytosolic DNA and depends on STING. A, BC2 cells were transfected with 4 μg Alexa-488-labeled MSCV-IRES-*Gfp* plasmid DNA, C57BL/6 genomic DNA, or ssDNA. Some cells were treated with 10 μmol/L Ara-C or DMSO. Sixteen hours later, BC2 cells were stained for indicated NKG2DLs and analyzed by flow cytometry. Bold line, Ara-C–treated or Alexa-488$^+$ cells; dashed line, Alexa-488$^-$ or DMSO-treated cells; fine line, isotype staining of Ara-C–treated or Alexa-488$^+$ cells; dotted line, isotype staining of Alexa-488$^-$ cells; filled histograms, isotype staining of DMSO-treated cells. B, MEFs expressing nonfunctional or WT *Sting* were transduced with retroviral vectors encoding *Sting* or empty vector. Eight days after selection, cells were treated with 10 μmol/L Ara-C for 16 hours (bold line) or DMSO (fine line) and stained for indicated NKG2DLs. Isotype stainings of DMSO (filled histogram) or Ara-C–treated cells (dashed line) are shown. C, *Sting*-, *Zbp1/Dai*- and *Rig-I*–specific (bold line) or control shRNAs-transduced (fine line) BC2 cells were treated with 10 μmol/L Ara-C for 16 hours. Gene-specific (dashed line) or control shRNA-transduced (dotted line) BC2 cells were also treated with DMSO for 16 hours. NKG2DL expression was analyzed by flow cytometry. Filled histograms, isotype staining of Ara-C–treated cells. D, *Sting*-, *Zbp1/Dai*-, and *Rig-I*–specific (bold lines) or control shRNA-transduced (fine line) Yac-1 cells were stained for NKG2DL expression. Isotype staining of gene-specific (dashed line) or control shRNA (filled histogram)-transduced Yac-1 cells is shown. MFI ± SD are indicated.

IRF3 (8). We therefore tested whether STING is necessary for RAE1 expression in cells exposed to genotoxic stress. MEFs harboring a loss-of-function *Sting* mutation failed to upregulate RAE1 in response to Ara-C (Fig. 6B). Reconstitution of *Sting* expression resulted in restored inducibility of RAE1 in the cells. Furthermore, RAE1 induction by Ara-C was impaired in BC2 cells expressing a *Sting*-specific shRNA (Fig. 6C) and *Sting* inhibition in Yac-1 cells resulted in reduced constitutive RAE1 expression (Fig. 6D).

Next, we tested the requirement in RAE1 induction for one candidate STING-dependent DNA sensor, ZBP/DAI, that activates IRF3 (8). Knockdown of *Zbp1/Dai* partly inhibited the upregulation of RAE1αβγ in response to Ara-C, but had little effect on RAE1βδ (Fig. 6C). In contrast, knockdown of *Zbp1/Dai* modestly inhibited RAE1βδ but not RAE1αβγ expression in Yac-1 cells (Fig. 6D). Inhibition of *Rig-I*, a RNA sensor that may indirectly mediate responses to cytosolic DNA, had no effect on RAE1 expression in BC2 or Yac-1 cells (Fig. 6C and D). Hence, DNA sensors other than ZBP1/DAI are likely to participate in inducing RAE1 expression in response to DNA damage, in line with other evidence suggesting the existence of DNA sensors that act redundantly (30). Taken together, these data suggest that cytosolic DNA sensor pathways regulate RAE1 expression in cells exposed to DNA damage.

IRF3 regulates RAE1 expression in B-cell lymphomas of Eμ-*Myc* mice

To address whether IRF3 regulates RAE1 expression in lymphomas, *Irf3*-deficient mice were bred to mice overexpressing c-*Myc* under the control of immunoglobulin heavy-chain enhancer region (Eμ), analogous to human Burkitt lymphoma (31). Spontaneous B220^{low} B-cell lymphomas develop by 15 to 20 weeks of age and the progression of lymphomas is accelerated in NKG2D$^{-/-}$;Eμ-*Myc* mice (4, 32). Tumor cells in Eμ-*Myc* mice express phosphorylated ATM (ATMpS1981; Fig. 7A; ref. 19). Staining of tumor cells with a dsDNA-specific antibody revealed the presence of cytosolic dsDNA in B220^{low} tumor cells, but not normal B220$^+$ B cells (Fig. 7B). The accumulation of cytosolic DNA was strictly dependent on the DDR as administration of the ATM inhibitor KU55933 resulted in reduced levels of cytosolic dsDNA (Fig. 7C). *Irf3*$^{+/-}$;Eμ-*Myc* mice (median survival = 62 days) experienced a significantly reduced survival rate compared with *Irf3*$^{+/+}$;Eμ-*Myc* mice (median survival = 116 days; Fig. 7D). We were not able to generate *Irf3*$^{-/-}$;Eμ-*Myc* mice because *Irf3*$^{+/-}$;Eμ-*Myc* mice failed to breed. Heterozygosity of *Irf3* in Eμ-*Myc* mice resulted in 2.5-fold decrease of IRF3 levels and reduced expression of IRF3 target genes in splenic B-cell lymphomas when compared with *Irf3*$^{+/+}$;Eμ-*Myc* mice, suggesting that cytosolic DNA in

Published OnlineFirst March 3, 2014; DOI: 10.1158/0008-5472.CAN-13-1703

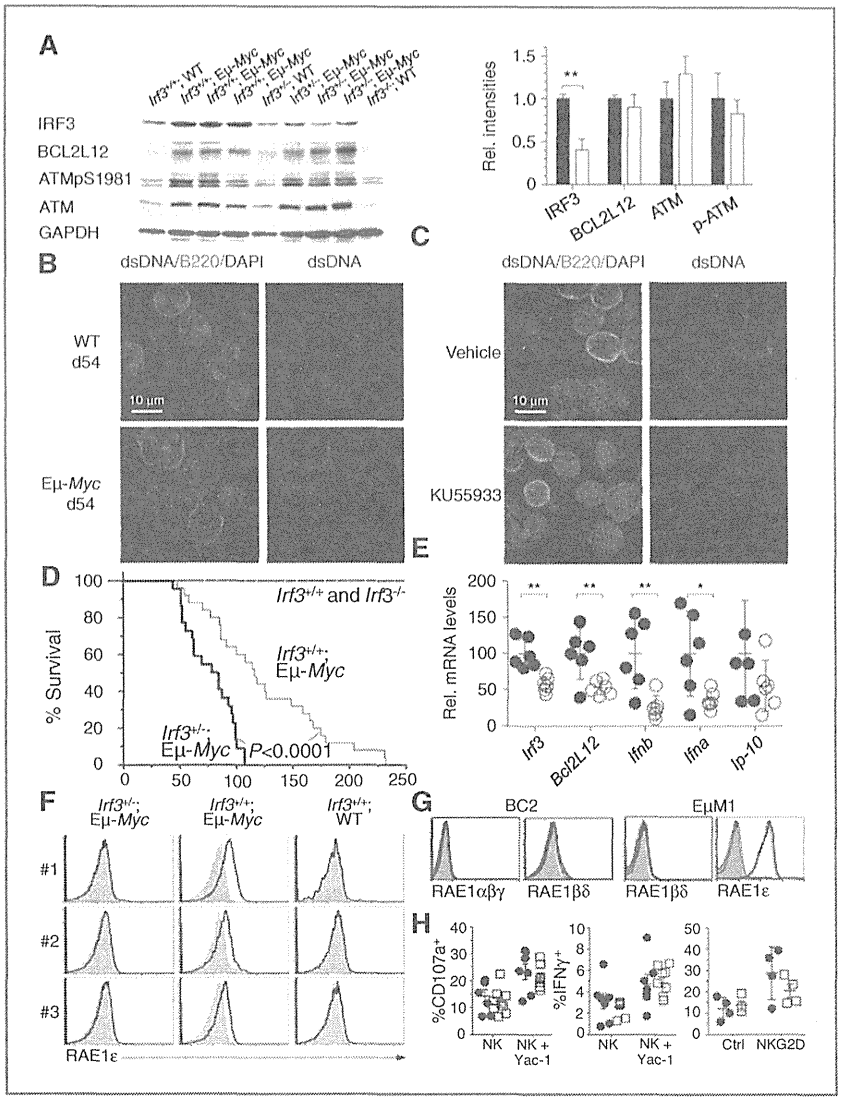

Figure 7. RAE1 expression in c-*Myc*-driven lymphomas depends on IRF3. A, immunoblot analysis of splenic B-cell lymphomas (>78% purity) from *Irf3*$^{-/-}$;Eμ-*Myc*, *Irf3*$^{+/+}$;Eμ-*Myc*, *Irf3*$^{+/+}$;WT, *Irf3*$^{-/-}$;WT, and *Irf3*$^{-/-}$;WT probed with antibodies for IRF3, BCL2L12, ATM, ATMpS1981, and GAPDH (left). Densitometry analysis of immunoblots showing mean ±SD from three mice normalized to GAPDH levels; **, $P < 0.01$. B, B220^{+} (green) cells of WT and Eμ-*Myc* mice were stained for dsDNA (red) in the presence of DAPI (blue) at 54 days of age. C, Eμ-*Myc* mice were injected intraperitoneally with 5 mg/kg KU55933 ($n = 3$) or vehicle ($n = 3$) at 34 and 36 days of age and stained for dsDNA (red), B220 (green), and DAPI (blue) at 38 days of age. D, *Irf3*$^{-/-}$;Eμ-*Myc* mice (thick) exhibit decreased survival compared with *Irf3*$^{+/+}$;Eμ-*Myc* (thin line), nontransgenic (dashed line), or *Irf3*$^{-/-}$ (dotted line) mice. The Kaplan–Meier analysis of survival of *Irf3*$^{+/+}$;Eμ-*Myc* mice ($n = 25$; median survival, 116 days), *Irf3*$^{+/-}$;Eμ-*Myc* mice ($n = 17$; median survival, 62 days), and *Irf3*$^{+/+}$ or *Irf3*$^{-/-}$ mice ($n = 25$; median survival, >250 days). $P < 0.0001$ by log-rank test or by the Gehan–Breslow–Wilcoxon test. E, relative mRNA levels of indicated IRF3 target genes in purified tumor cells of *Irf3*$^{-/-}$;Eμ-*myc* and *Irf3*$^{+/+}$;Eμ-*Myc* mice were measured by qRT-PCR. F, RAE1ε expression in tumor cells of three *Irf3*$^{+/-}$;Eμ-*Myc* mice. B220^{low} cells in blood of moribund *Irf3*$^{+/-}$;Eμ-*Myc*, *Irf3*$^{+/+}$;Eμ-*Myc*, and C57BL/6 mice (bold line) were stained for the indicated NKG2D ligand expression. Filled histogram, isotype staining of B220^{low} tumors. G, *Bcl2l12*-IRES-*Gfp* (red line) or IRES-*Gfp*–transduced (blue line) BC2 (left) or EμM1 (right) cells were stained for the indicated NKG2DLs 3 days posttransduction. Dashed line, isotype staining of *Bcl2l12*-IRES-*Gfp*–transduced cells. Fine line, isotype staining of IRES-*Gfp*–transduced cells. Filled histograms, isotype staining of untransduced cells. H, IL-2–activated NK cells derived from *Irf3*$^{+/-}$;Eμ-*Myc* (white squares, $n = 8$) or *Irf3*$^{+/+}$;Eμ-*Myc* (black circles, $n = 7$) mice were cocultured with Yac-1 cells at an effector to target ratio of 3:1. After 4 hours, the percentage of CD107a and IFN-γ–expressing NK1.1^{+}CD3^{-} cells was determined by flow cytometry (left and middle). Freshly isolated splenocytes of *Irf3*$^{+/-}$;Eμ-*Myc* (white squares, $n = 4$) and *Irf3*$^{+/+}$;Eμ-*Myc* (black circles, $n = 4$) mice were stimulated *in vitro* for 5 hours on plates coated with NKG2D-specific antibodies (MI-6, 10 μg/mL) or isotype control (10 μg/mL) before staining and analysis. Intracellular IFN-γ was detected by flow cytometry gated on NK1.1^{+}CD3^{-} cells (right). Error bar denotes SE of mean.

Published OnlineFirst March 3, 2014; DOI: 10.1158/0008-5472.CAN-13-1703

lymphomas activates IRF3 (Fig. 7A and E). Importantly, reduced levels of IRF3 in lymphomas impaired RAE1ε expression, the only RAE1 family member detected in Eμ-*Myc* tumor cells (Fig. 7F; ref. 33).

The null mutation introduced into the *Irf3* allele also resulted in functional inactivation of the neighboring *Bcl2l12* gene, which promotes or suppresses tumorigenesis depending on the cellular context (34, 35). However, heterozygosity of the gene-targeted locus did not result in reduced BCL2L12 levels or changes in the rate of apoptosis or proliferation of lymphomas (Supplementary Figs. S7A and S7B; Fig. 7A). Overexpression of *Bcl2l12* in BC2 and EμM1 cells, two cell lines derived from Eμ-*Myc* mice, had no effect on RAE1 expression, proliferation, or apoptosis (Fig. 7G; Supplementary Figs. S7C and S7D). We previously found that NK cells and T cells contribute to immunosurveillance in Eμ-*Myc* mice (18). However, *Irf3* deficiency had no impact on NK- and T-cell numbers or NK cell activity (Fig. 7H; ref. 36). In summary, our data suggest that RAE1 ligands are regulated by IRF3 in lymphomas of Eμ-*Myc* mice. Interestingly, IRF3 is likely to have additional functions in immunosurveillance as NKG2D deficiency increases the tumor load of Eμ-*Myc* mice, but has no impact on survival (4).

Discussion

Our previous results provided evidence that the DDR activates immune responses by inducing NKG2DLs (6). Here, we show that cytosolic DNA contributes to the induction of RAE1 expression in lymphoma cells in response to DNA damage for the following reasons: (i) inhibition of the DDR impaired the induction of cytosolic DNA and RAE1 molecules; (ii) transfection of DNA into cells upregulated RAE1 expression; (iii) inhibition of STING, TBK1, or IRF3 impaired RAE1 expression; (iv) TBK1 and IRF3 were activated in response to DNA damage in a DDR-dependent manner; and (v) overexpression of TBK1 or IKKε induced RAE1 expression.

Linking the DDR to STING-initiated pathways is of interest immunologically, because STING is a critical component of a major pathway common to receptors that detect cytosolic DNA and RNA of pathogens (8). Previous studies provided indications that the DDR induces phosphorylation of IRF3 and that certain Toll-like receptor agonists induce *Raet1* gene expression in peritoneal macrophages (37), but the linkage of these pathways had not been explored. Much remains to be determined about the relation of the DDR and STING pathways. We observed less phosphorylation of IRF3 in response to DNA damage when compared with LPS, suggesting that IRF3 translocation and transcriptional activity is differentially regulated in response to DNA damage. Consistent with this possibility, Noyce and colleagues reported that no minimal posttranslational modification of IRF3 correlated with its transcriptional activity (38). Of interest was that DNA damage consistently led to lower induction of IFN than Poly I:C. The reduced induction likely reflects the fact that the DDR failed to induce IRF7 activation, which is necessary for efficient transcription of IFN genes (data not shown).

Cytosolic DNA has been shown to be present in cells upon infection or the uptake of apoptotic cells (8). Our data show the presence of cytosolic DNA in uninfected lymphoma cell lines. An intriguing question is where cytosolic DNA originates from and the mechanism leading to cytosolic DNA in tumor cells. DNA damage is known to induce transcription of retroelements, including transposases, derived from functional endogenous retrovirus present in the genome (39). Alternatively, cytosolic DNA could be generated during DDR-dependent DNA repair that can result in deletion of genomic DNA.

An important question is the nature of the DNA sensor recognizing the cytosolic DNA. The induction of RAE1 by Ara-C partially relied on ZBP1/DAI. ZBP1/DAI is a candidate sensor that is reported to activate TBK1/IRF3 (40). However, additional TBK1-activating DNA sensors exist as MEFs from *Zbp1*$^{-/-}$-deficient mice mount a normal type I IFN response to DNA (18, 30). These sensors may be required for constitutive RAE1 expression in Yac-1 cells. Hence, unidentified DNA sensors may play a predominant role in YAC-1 cells, or may function redundantly with ZBP1/DAI, in the induction of RAE1.

NKG2D plays an important role in immunosurveillance of tumors in Eμ-*Myc* mice (4, 5). The accelerated development of lymphoma in *Irf3/Bcl2l12*$^{+/-}$;Eμ-*Myc* mice when compared with NKG2D-deficient mice suggests that IRF3 induces the expression of molecules other than RAE1 ligands important for immunosurveillance or suppression of tumorigenesis. IRF3 and BCL2L12 are known to induce genes implicated in apoptosis (11). However, we observed no differences in the rates of apoptosis or proliferation comparing WT and heterozygous tumor cells, suggesting that accelerated tumorigenesis of *Irf3/Bcl2l12*$^{+/-}$;Eμ-*Myc* mice is not due to effects of IRF3 or BCL2L12 on apoptosis or proliferation. In summary, our data suggest that tumorigenesis leads to accumulation of cytosolic DNA and subsequent activation of an antitumor immune response that may partially depend on NKG2D.

Disclosure of Potential Conflicts of Interest

No potential conflicts of interest were disclosed.

Authors' Contributions

Conception and design: A.R. Lam, N.L. Bert, D.H. Raulet, S. Gasser
Development of methodology: A.R. Lam, N. Le Bert, S.S. Ho, Y.J. Shen, C.X. Koo, S. Gasser
Acquisition of data (provided animals, acquired and managed patients, provided facilities, etc.): A.R. Lam, N. Le Bert, S.S. Ho, Y.J. Shen, M.L.F. Tang, G.M. Xiong, J.L. Croxford, C.X. Koo, K.J. Ishii, S. Gasser
Analysis and interpretation of data (e.g., statistical analysis, biostatistics, computational analysis): A.R. Lam, N. Le Bert, S.S. Ho, Y.J. Shen, M.L.F. Tang, C.X. Koo, K.J. Ishii, D.H. Raulet, S. Gasser
Writing, review, and/or revision of the manuscript: A.R. Lam, N. Le Bert, Y.J. Shen, D.H. Raulet, S. Gasser
Administrative, technical, or material support (i.e., reporting or organizing data, constructing databases): A.R. Lam, S. Akira
Study supervision: A.R. Lam, K.J. Ishii, S. Gasser

Grant Support

This work was supported by Biomedical Research Council grant 07/1/21/19/513, National Research Foundation grant HUJ-CREATE-Cellular and Molecular Mechanisms of Inflammation, and by grants from the US NIH to D.H. Raulet.

The costs of publication of this article were defrayed in part by the payment of page charges. This article must therefore be hereby marked *advertisement* in accordance with 18 U.S.C. Section 1734 solely to indicate this fact.

Received June 18, 2013; revised January 14, 2014; accepted February 1, 2014; published OnlineFirst March 3, 2014.